Materials Science and Engineering R 73 (2012) 51–65

Contents lists available at SciVerse ScienceDirect

Materials Science and Engineering R

journal homepage: www.elsevier.com/locate/mser

Recent progress in cathode materials research for advanced lithium ion batteries

Bo Xu, Danna Qian, Ziying Wang, Ying Shirley Meng *

Department of NanoEngineering, University of California San Diego, La Jolla, CA 92093, USA

ARTICLE INFO

Article history:
Available online 5 June 2012

ABSTRACT

New and improved materials for energy storage are urgently required to make more efficient use of our finite supply of fossil fuels, and to enable the effective use of renewable energy sources. Lithium ion batteries (LIB) are a key resource for mobile energy, and one of the most promising solutions for environment-friendly transportation such as plug-in hybrid electric vehicles (PHEVs). Among the three key components (cathode, anode and electrolyte) of LIB, cathode material is usually the most expensive one with highest weight in the battery, which justifies the intense research focus on this electrode. In this review, we present an overview of the breakthroughs in the past decade in developing high energy high power cathode materials for lithium ion batteries. Materials from six structural groups (layered oxides, spinel oxides, olivine compounds, silicate compounds, tavorite compounds, and borate compounds) are covered. We focus on their electrochemical performances and the related fundamental crystal structures, solid-state physics and chemistry are covered. The effect of modifications on both chemistry and morphology are discussed as well.

Contents

1. Introduction

With the worldwide energy shortage being one of the mounting problems in 21st century, efforts have been made to replace the non-renewable fossil fuels by other green energy sources, such as solar, wind, and hydroelectric power. Different from the conventional fossil fuels, most of these green energy sources suffer from their uncontrollable and intermittent nature, therefore the difficulty in energy storage and regulation results in larger cost. This brings in enormous amount of research interests in material developments for energy storage. The LIB system is regarded as one of the near-term solutions because of its high energy density and relatively simple reaction mechanism. Current LIB technology is well developed for the portable electronic devices and has been widely used in the past twenty years. However, to be implemented in the large-scale high-power system such as the plug-in hybrid electric vehicle (PHEV) or plug-in electric vehicle (PEV), performance requirements are raised especially from the aspects of energy/power density, cycling life and safety issues, therefore further LIB material and system developments are necessary.

The basic working principles of LIB are shown in Fig. 1. A lithium ion battery can work as the energy storage device by converting electric energy into electrochemical energy. There are three key components in a LIB system: cathode, anode and electrolyte. For today's commercialized LIB system, both cathode and anode materials are intercalation materials. The transition metal oxides in cathode (graphite in anode) consist of a largely unchangeable host with specific sites for Li ions to be intercalated in. All Li ions

* Corresponding author.
E-mail address: shirleymeng@ucsd.edu (Y.S. Meng).

0927-796X/$ – see front matter © 2012 Elsevier B.V. All rights reserved.
http://dx.doi.org/10.1016/j.mser.2012.05.003

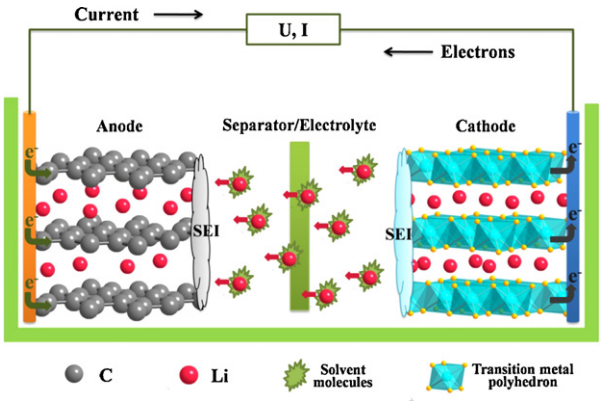

Fig. 1. Working principles of LIB (charging).

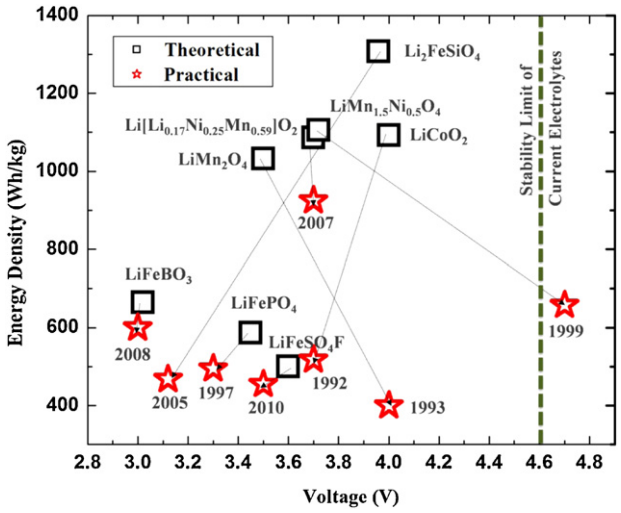

Fig. 2. Theoretical and practical gravimetric energy densities of different cathode materials.

are in the cathode sides initially and the battery system is assembled in "discharged" status. While charging, Li ions are extracted from the cathode host, solvate into and move through the non-aqueous electrolyte, and intercalate into the anode host. Meanwhile, electrons also move from cathode to anode through the outside current collectors forming an electric circuit. The chemical potential of Li is much higher in the anode than in the cathode, thus the electric energy is stored in the form of (electro)chemical energy. Such process is reversed when the battery is discharging where the electrochemical energy is released in the form of electric energy. The cathode region and anode region are separated by the separator, a micro-porous membrane that allows the electrolyte to penetrate and prevent shorting between the two electrodes. The electrolyte should be ionically conducting and electronically insulating in principle, however the actual properties of the electrolyte is much more complicated. During the first cycle, a so-called solid–electrolyte-interphase (SEI) layer will be formed on the surface of electrodes due to the decomposition of organic electrolyte at extreme voltage range (typically <1.2 V or >4.6 V). In current LIB technology, the cell voltage and capacities are mainly determined by the cathode material that is also the limiting factor for Li transportation rate. The developments of cathode materials therefore become extremely crucial and receive much attention in recent decade.

Since 1980 when the $LiCoO_2$ was demonstrated firstly as a possible cathode material for rechargeable lithium battery [1], the transition metal intercalation oxides have caught the major research interests as the LIB cathodes [2–8]. Categorized by structure, the conventional cathode materials include layered compounds $LiMO_2$ (M = Co, Ni, Mn, etc.), spinel compounds LiM_2O_4 (M = Mn, etc.), and olivine compounds $LiMPO_4$ (M = Fe, Mn, Ni, Co, etc.). Most of the researches are performed on these materials and their derivatives. New structure intercalation materials such as silicates, borates and tavorites are also gaining increasing attentions in recent years. During the materials optimization and development, following designing criterions are often considered: (1) energy density; (2) rate capability; (3) cycling performance; (4) safety; (5) cost. The energy density is determined by the material's reversible capacity and operating voltage, which are mostly determined by the material intrinsic chemistry such as the effective redox couples and maximum lithium concentration in active materials. For rate capability and cycling performances, electronic and ionic mobilities are key determining factors, though particle morphologies are also important factors due to the anisotropic nature of the structures and are even playing a crucial role in some cases. Therefore materials optimizations are usually made from two important aspects, to change the intrinsic chemistry and to modify the morphology (surface property, particle size, etc.) of the materials. Fig. 2 compares the gravimetric energy densities of different cathode materials that are currently under investigations. While some materials such as $LiFeBO_3$ and $LiFeSO_4F$ are already approaching their theoretical energy densities, for other materials including conventional layered and spinel compounds, significant gaps are still present between their theoretical and practical energy densities. The materials with promising theoretical properties have high potentials as the candidates of future generation LIB cathode, therefore are under intensive studies. For certain materials such as the $LiFePO_4$ olivine, significant property improvements have been achieved during the past decade with assistance of newly developed technologies. To review and summarize those researches could provide inspiring perspectives for further material optimizations. In this review, we will discuss the recent research progress in the past decade of different cathode materials following the structural category, and modifications on both chemistry and morphology will be discussed.

2. Layered compounds $LiMO_2$

The ideal structure of layered compound $LiMO_2$ is demonstrated in Fig. 3. The oxygen anions (omitted for clarity in the figures) form a close-packed *fcc* lattice with cations located in the 6-coordinated octahedral crystal site. The MO_2 slabs and Li layers are stacked alternatively. Although the conventional layered oxide $LiCoO_2$ has been commercialized as the LIB cathode for twenty years, it can only deliver about 140 mAh/g capacity which is half of its theoretical capacity. Such limitation can be attributed to the intrinsic structural instability of the material when more than half

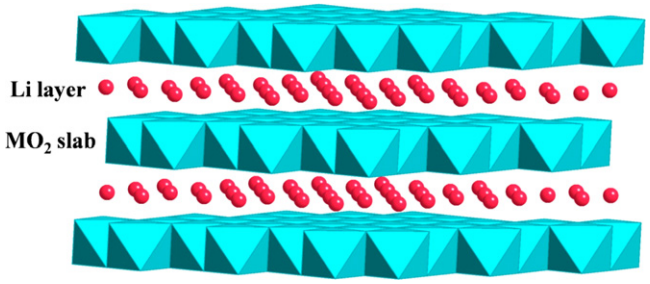

Fig. 3. Crystal structure of layered $LiMO_2$ (blue: transition metal ions; red: Li ions). (For interpretation of the references to color in this figure legend, the reader is referred to the web version of the article.)

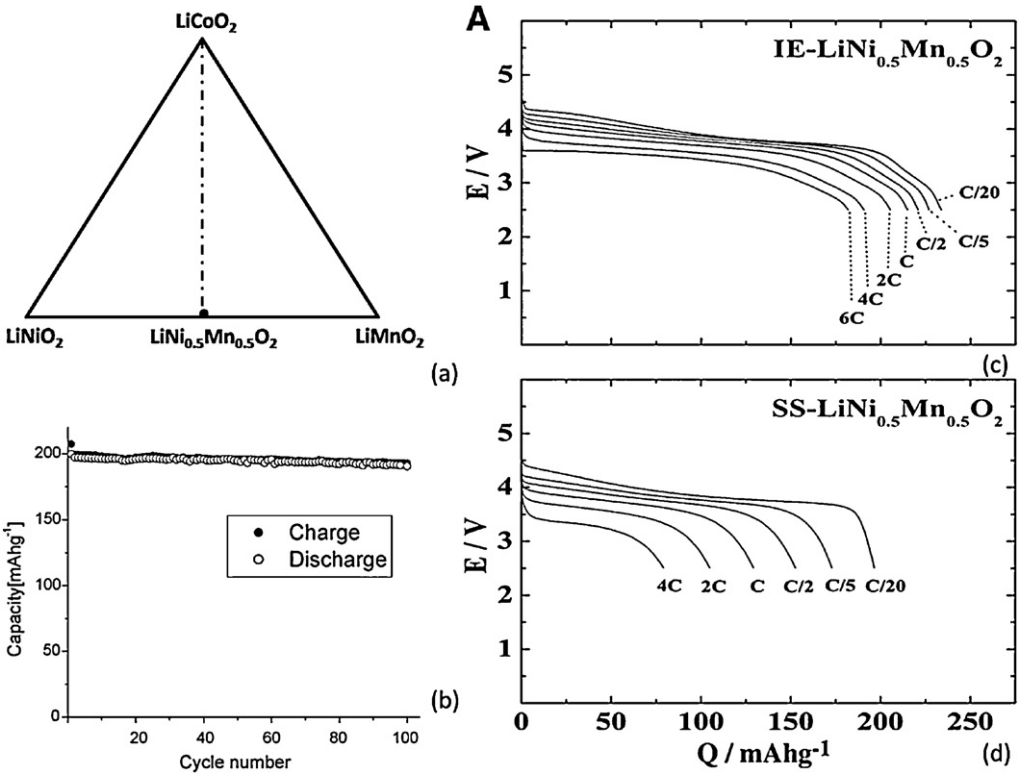

Fig. 4. Performance of layered $LiNi_{0.5}Mn_{0.5}O_2$: (a) compositional phase diagram, (b) cycling performance [10], (c) rate performance of $LiNi_{0.5}Mn_{0.5}O_2$ synthesized by ion-exchange method [11], and (d) rate performance of $LiNi_{0.5}Mn_{0.5}O_2$ synthesized by solid state method [11].

of the Li ions are extracted. On the other hand, the presence of toxic and expensive Co ions in $LiCoO_2$ has introduced the environmental problem as well as raised the cost of the LIB. The research focusing on layered compounds, therefore have moved from $LiCoO_2$ to its derivatives in which Co ions are partially/fully substituted by more abundant and environmental friendly transition metal ions, such as Ni and Mn. The approaches include mixing the $LiNiO_2$ and $LiMnO_2$ with 1:1 ratio, forming layered $LiNi_{0.5}Mn_{0.5}O_2$, and the formation of Li–Co–Ni–Mn–O layered compound (so-called NMC type materials).

Good electrochemical data of $LiNi_{0.5}Mn_{0.5}O_2$ was firstly reported in 2001 by Ohzuku et al. [9]. Fig. 4 shows the typical electrochemical performance of $LiNi_{0.5}Mn_{0.5}O_2$ [10,11]. The charge/discharge voltages of this material are around 3.6–4.3 V where Ni^{2+}/Ni^{4+} act as the redox couple as confirmed from in situ X-ray absorption spectroscopy (XAS) study [12]. Various methods including X-ray and neutron diffraction, nuclear magnetic resonance (NMR) spectroscopy, transmission electron microscope (TEM) and first-principles calculations [13–18] have been performed to investigate the structural change and local cation distribution of this material. The results showed that different from classic layered material composed of pure Li layer and pure MO_2 slab, 8–10% Ni ions are usually found in the Li layer of $LiNi_{0.5}Mn_{0.5}O_2$ synthesized by solid state or sol–gel synthesis methods. It was suggested that such Li–Ni interlayer mixing might be partially reduced under high voltage (>4.6 V) [19,20]. For the transition metal layer, a flower-like in-plane cation ordering that Li in transition metal layer is surrounded sequentially by Mn rings and Ni rings was suggested by first-principles calculations [16] and confirmed by experiments [14,15]. With MO_2 slabs pined together by the Ni in Li layer, larger reversible capacity (~200 mAh/g) can be obtained in $LiNi_{0.5}Mn_{0.5}O_2$ at low rate (*C*/20) with little capacity fading even after 100 cycles, therefore the energy density can be significantly improved. The material structure is thermally stable until ~300 °C, above which oxygen release and material decomposition would occur [21]. Structural change including migration of transition metal ions to Li layer at high temperature was also reported both experimentally and computationally [21,22]. However, with large amount of un-removable Ni in the Li layers blocking Li diffusion pathways, the Li mobility of the materials is negatively affected. The Li diffusion coefficient in $LiNi_{0.5}Mn_{0.5}O_2$ is reported to be lower than that in $LiCoO_2$ by one magnitude of order [23], resulting in the low rate capability of $LiNi_{0.5}Mn_{0.5}O_2$. It was also reported by Kang et al. [11] that the Li–Ni exchange is reduced to ~4% in $LiNi_{0.5}Mn_{0.5}O_2$ synthesized by ion-exchange method, therefore the rate capability can be significantly improved (shown in Fig. 4(c) and (d)).

Considering the Li–Ni disorder being major factor affecting the material rate capability, attempts to create new compounds of $LiCo_xNi_yMn_{1-x-y}O_2$ are motivated. While good electrochemical performance of $LiCo_{1/3}Ni_{1/3}Mn_{1/3}O_2$ was already reported in 2001 by Ohzuku et al. [24], the importance of the series of Li–Co–Ni–Mn–O material is more recognized as the presence of Co ions can help to reduce the amount of defect Ni in Li layer. The $LiCo_{1/3}Ni_{1/3}Mn_{1/3}O_2$ layer compound can be regarded as the solid solution of $LiCoO_2$, $LiNiO_2$ and $LiMnO_2$. $LiCo_{1/3}Ni_{1/3}Mn_{1/3}O_2$ deliver similar reversible capacity with $LiNi_{0.5}Mn_{0.5}O_2$. Their voltage profile are also similar in shape, but the operation voltage window of $LiCo_{1/3}Ni_{1/3}Mn_{1/3}O_2$ can be extended to 3.6–4.7 V. The material's typical electrochemical performance is shown in Fig. 5 [25,26]. With additional Co ions existing in the structure, the Li–Ni interlayer mixing can be much reduced to 1–6% [27–32]. Though certain superlattice in the transition metal layer could be obtained from computations [33,34], diffraction [28] and NMR study [35], it is suggested that only short-range ordering can be found and Li in transition metal layer is surrounded primarily by Mn ions. The changes of transition metal valence state following cycling were investigated experimentally and computationally [29,30,32,34–36]. In general, it is believed that, the transition metal ions are oxidized in sequence of Ni^{2+} to Ni^{3+}, Ni^{3+} to Ni^{4+}, Co^{3+} to Co^{4+}

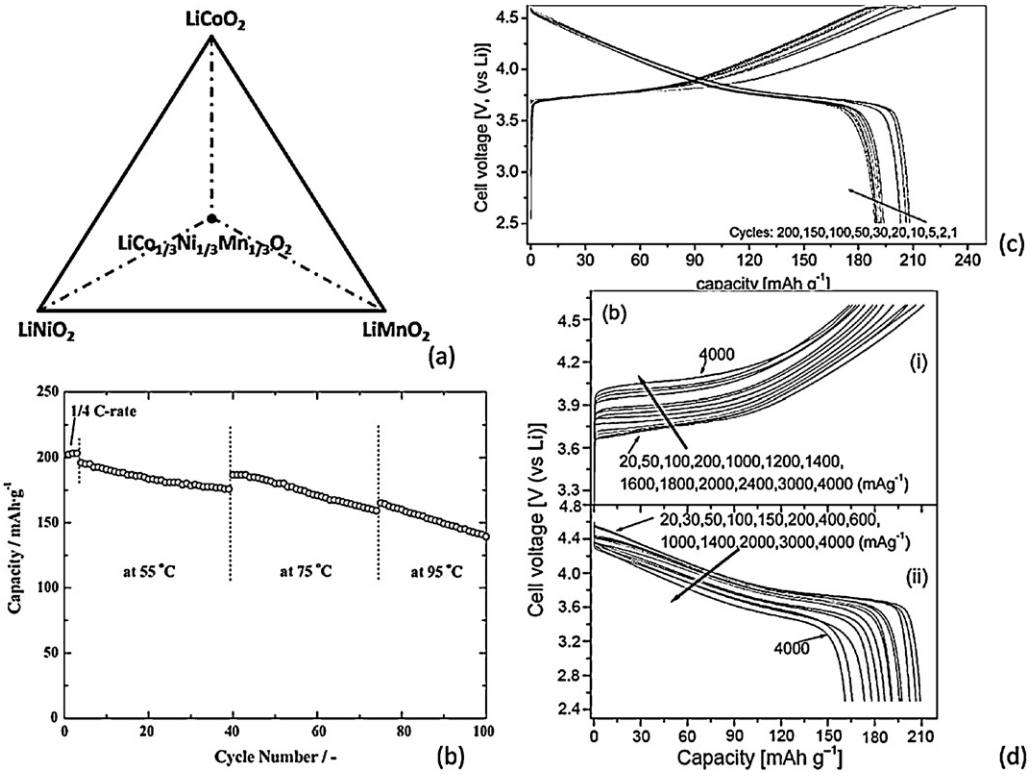

Fig. 5. Performance of layered $LiCo_{1/3}Ni_{1/3}Mn_{1/3}O_2$: (a) compositional phase diagram, (b) cycling performance at elevated temperatures [25], (c) cycling performance at room temperature [26], and (d) rate performance at room temperature [26].

during charging. Mn^{4+} ions keep unchanged. However, due to the overlap of oxygen 2p band $M^{3+/4+}$ band, at the end of charging, part of the electrons were also removed from the oxygen ions, causing possible oxygen release at high charging voltages (>4.5 V). As shown in Fig. 5(c) and (d), with certain morphology modifications, ~90% of the capacity can be retained after 200 cycles at room temperature and 84% of the capacity can be retained when at a discharge rate as high as 20*C* [26]. The $LiCo_{1/3}Ni_{1/3}Mn_{1/3}O_2$ compound also shows relatively good performance at elevated temperatures. It was reported [25] that more than 80% capacity can be retained at 55 °C and half of the capacity can still be achieved when the operation temperature is raised to 95 °C. We also want to point out that the reduced amount Co can be used to achieve the same benefits. It has been shown by Li et al. that as little as 20% Co ($LiCo_{0.2}Ni_{0.4}Mn_{0.4}$) can lead to excellent electrochemical performance [37].

While the introduction of Co ions into $LiNi_{0.5}Mn_{0.5}O_2$ could improve the material stability, the introduction of extra Li ions, on the other hand, could improve the material capacity. A series of Li-rich layered oxides $Li[Li_{1/3-2x/3}Ni_xMn_{2/3-x/3}]O_2$ therefore are created by making a compound between Li_2MnO_3 and $LiNi_{0.5}Mn_{0.5}O_2$ to achieve higher capacity beyond the limitation of one Li ion per MO_2 formula. With excess Li ions introduced, the theoretical capacity of this series of materials can be increased to more than 300 mAh/g. The compound $Li[Li_{1/9}Ni_{1/3}Mn_{5/9}]O_2$ is firstly reported by Lu et al. in 2001 [17]. Different compositions (x = 1/6, 1/5, 1/4, 1/3, 5/12, etc.) of this series of materials were studied by the same group later and similar electrochemical performances were shown [38]. For this series of materials, the pristine samples are solid solutions phase following the layered structure in general, although it was reported that some of the spinel feature might be observed when $x \geq 1/3$ being heated to 600 °C [38]. The Li–Ni interlayer mixing is usually much smaller than that in $LiNi_{0.5}Mn_{0.5}O_2$. With x increasing, the Li–Ni interlayer mixing also increases while the c/a ratio decreases. The structure details and cation ordering were investigated by diffraction, TEM, NMR spectroscopy and first-principles calculations [39–44]. The results show that the excess Li ions were located in the transition metal layer, surrounded mostly by 5 or 6 Mn^{4+} ions. The Ni/Mn zigzag ordering is regarded as another competent driving force for the in-plane cation ordering, and actual material may reflect a combination of these two orderings [39]. A typical voltage profile of $Li[Li_{1/9}Ni_{1/3}Mn_{5/9}]O_2$ for the first cycle charging is shown in Fig. 6(c) [45]. It is composed of a slopy region from the open circuit voltage to ~4.5 V followed by a plateau region between 4.5 V and 4.6 V. Such plateau, however, does not appear in following cycles causing a large first cycle irreversible capacity. While it is generally agreed that the slopy region originates from the oxidization of Ni^{2+} to Ni^{4+}, the mechanism of the anomalous high voltage capacity is still under debate. Several studies [46–48] proposed the mechanism of oxygen loss accompanied by Li removal, while other studies proposed the mechanisms involving surface reaction with electrode/electrolyte reduction [49] and/or hydrogen exchange [50]. This series of materials deliver the highest reversible capacity (>250 mAh/g) for current intercalation cathode materials, but only with low rate (*C*/50). It was reported that the excess Li ions in transition metal layer are electrochemically active and will migrate to Li layer becoming stable tetrahedral ions during cycling [44,51]. Recent study [44] also suggested a possible *layer to defective-spinel* phase transformation happening near the material surface with significant migration of transition metal ions to lithium layer. These un-removable ions in lithium layer will block the lithium diffusion pathways, therefore may be one of the reasons that cause the low Li chemical diffusion coefficient in the plateau region [43] and the intrinsic poor rate capability of this series of materials. A recent study also suggested that the material rate and temperature performances may also be affected by the particle size as shown in Fig. 6 [45].

For the Li-rich layered compounds, the surface characteristics can significantly affect the material electrochemical performance

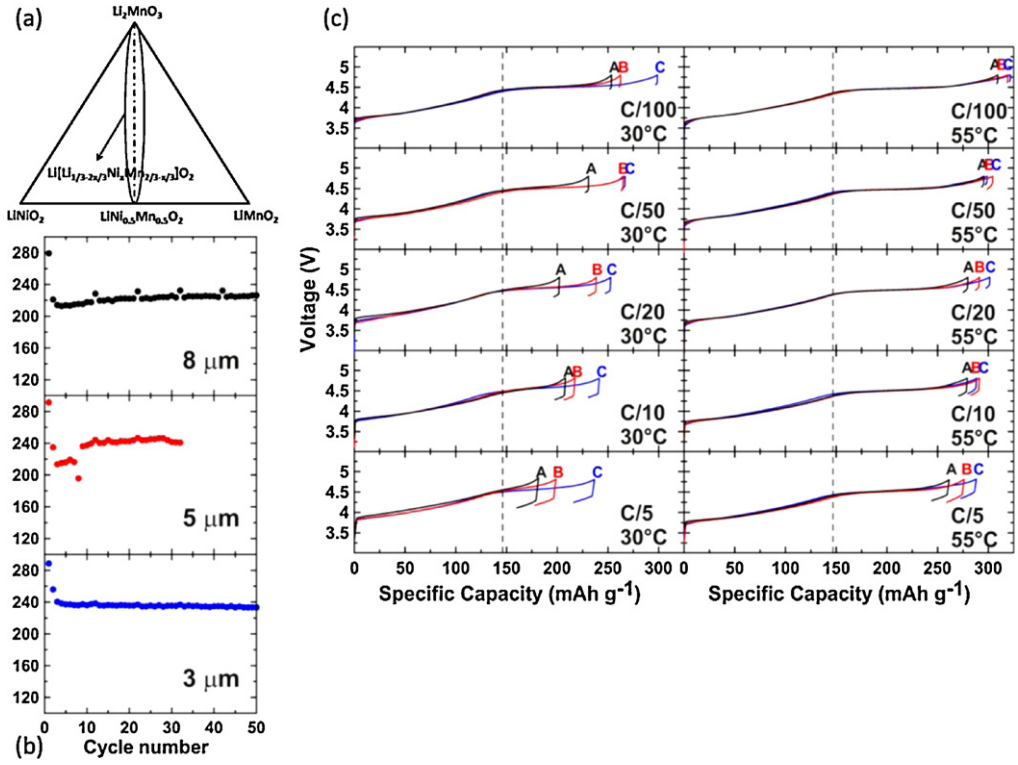

Fig. 6. Performance of layered $Li[Li_{1/3-2x/3}Ni_xMn_{2/3-x/3}]O_2$: (a) compositional phase diagram, (b) cycling performance ($x = 1/3$) [45], and (c) rate and temperature performance ($x = 1/3$) [45].

especially for the first-cycle irreversible capacity and rate capability. Different surface modifications, therefore, have been applied to this series of materials as further optimizations. Common coating materials applied include different types of metal oxides (Al_2O_3, Nb_2O_5, Ta_2O_5, ZrO_2, and ZnO) [52–54], metal fluorides AlF_3 [55,56] and other polyanion compounds such as MPO_4 (M = Al, Co) [57,58]. A systematic research on the metal oxides coating was performed by Myung et al. in 2007 [54]. The area-specific impedance (ASI) results showed that during the first cycle, the ASI of un-coated samples dramatically increased, while the ASI of all the coated samples hardly changed. The cycling performance and rate capabilities of the materials were improved especially when coated with Al_2O_3. It was claimed that during the initial cycling, the oxide coating reacted with the electrolyte forming a solid stable fluoride layer which protected the active materials from further HF scavenger. Similar effect was also reported for AlF_3 coating [56]. In addition, the coating can suppress the oxygen loss occurred in the active materials, therefore can also improve the material thermal stability [55,59]. The coating morphology is also under optimization. Double layer coating combing two or more coating materials has been developed as well [58]. Another approach involves the construction of composition gradient from surface to bulk and forming core–shell structured particles. The structure is shown in Fig. 7 [60]. By introducing composition gradient, the performance of "core" active materials can be maintained, while the less active "shell" materials can act as

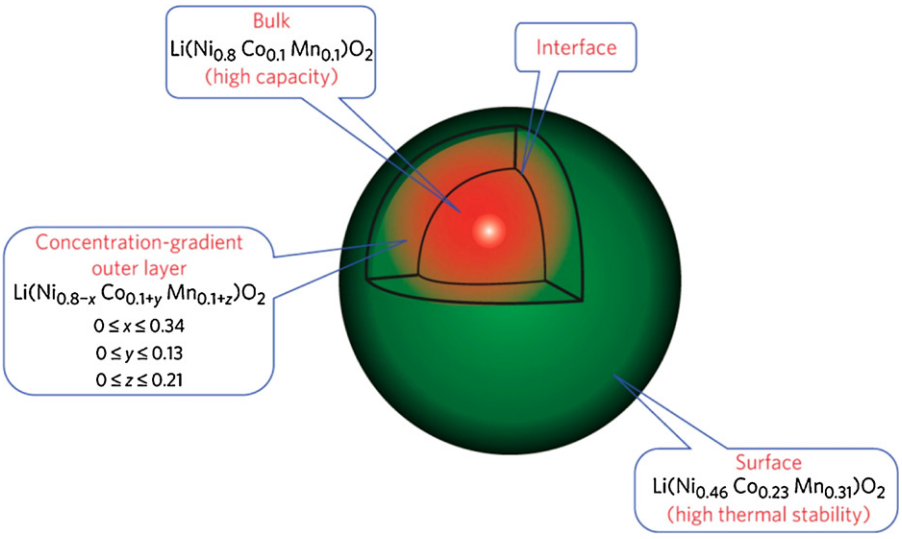

Fig. 7. Demonstration of core–shell structured particles [60].

a buffer layer and help improve the material performance in surface. Although there are general hypotheses of why the coating materials can improve the active materials' performance, the detailed mechanism is still unknown and under intensive investigations.

In summary, the layered oxides $LiMO_2$ can deliver high capacities after activation at high voltages, therefore leading to promising energy densities. However, their practical reversible capacities are usually limited by the intrinsic structural instability at low lithium concentrations and high voltages, causing reduced efficiency of the active material utilization. Besides, for the cobalt-free lithium nickel manganese oxides, the intrinsic low rate capability has become the bottleneck problem impeding the commercialization of these materials.

3. Spinel compounds LiM_2O_4

The structure of LiM_2O_4 spinel is shown in Fig. 8. The oxygen framework of LiM_2O_4 is the same as that of $LiMO_2$ layered structure. M cations still occupy the octahedral site but 1/4 of them are located in the Li layer, leaving 1/4 of the sites in transition metal layer vacant. Li ions occupy the tetrahedral sites in Li layer that share faces with the empty octahedral sites in the transition metal layer. The structure is based on a three-dimensional MO_2 host and the vacancies in transition metal layer ensure the three-dimensional Li diffusion pathways. The spinel $LiMn_2O_4$ was proposed as the cathode of the lithium ion battery by Thackeray et al. in 1983 [61–63], but the material was found to encounter sever capacity fading problem. Two reasons have been considered as the main sources for the capacity fading: (1) dissolution of Mn^{2+} into the electrolyte generated by the disproportional reaction 2 $Mn^{3+} \rightarrow Mn^{4+} + Mn^{2+}$ [64,65] and (2) generation of new phases during cycling and the related micro-strains [64,66]. Substituting Mn with other metal ions has been used as an important approach to improve cycling performance of spinel materials. Multiple dopants including inactive ions such as Mg, Al, and Zn [67–69], first row transition metal ions such as Ti, Cr, Fe, Co, Ni, and Cu [70–74] and rare earth metal ions such as Nd and La [75–77] have been investigated and $LiNi_{0.5}Mn_{1.5}O_4$ shows the best overall electrochemical performances among the above.

$LiNi_{0.5}Mn_{1.5}O_4$ follows the spinel structure of $LiMn_2O_4$ where Ni ions are located in the sites of Mn ions originally. With different synthesis conditions [78,79], $LiNi_{0.5}Mn_{1.5}O_4$ could possess two different structural symmetries, the ordered structure with space group $P4_332$ and the disordered structure with space group $Fd\bar{3}m$. In ordered $LiNi_{0.5}Mn_{1.5}O_4$, Ni ions occupy 4b sites and Mn ions occupy 12d sites forming an ordered pattern, while in disordered $LiNi_{0.5}Mn_{1.5}O_4$, Ni and Mn ions are randomly distributed in 16d sites. In stoichiometric $LiNi_{0.5}Mn_{1.5}O_4$, the valence of Ni ions is 2+ pushing all Mn ions to Mn^{4+}. Comparing to $LiMn_2O_4$ spinel, the redox couple of $LiNi_{0.5}Mn_{1.5}O_4$ is switched from Mn^{3+}/Mn^{4+} to Ni^{2+}/Ni^{4+} and the voltage is lifted from 4.1 V to 4.7 V. Such high discharge voltage not only enlarges the energy density but also makes the material capable to be coupled with anode materials which have better safety but relatively higher voltage ($Li_4Ti_5O_{12}$, etc.). However, phase-pure $LiNi_{0.5}Mn_{1.5}O_4$ is difficult to synthesize because impurities such as nickel oxides and/or lithium nickel oxides usually exist [78,80,81]. As an alternative approach, the off-stoichiometric material $LiNi_{0.5}Mn_{1.5}O_{4-x}$ which adopts the disordered structure is synthesized and the performances of these two materials are compared in Fig. 9 [71]. In $LiNi_{0.5}Mn_{1.5}O_{4-x}$, there are small amount of Mn^{3+} ions exist as the charge compensation of oxygen loss. The small voltage plateau ~4 V for $LiNi_{0.5}Mn_{1.5}O_{4-x}$ therefore is attributed to the Mn^{3+}/Mn^{4+} couple. Different from other doped spinel materials the voltage profile of which is usually composed of two distinct plateaus, there is only one flat plateau at

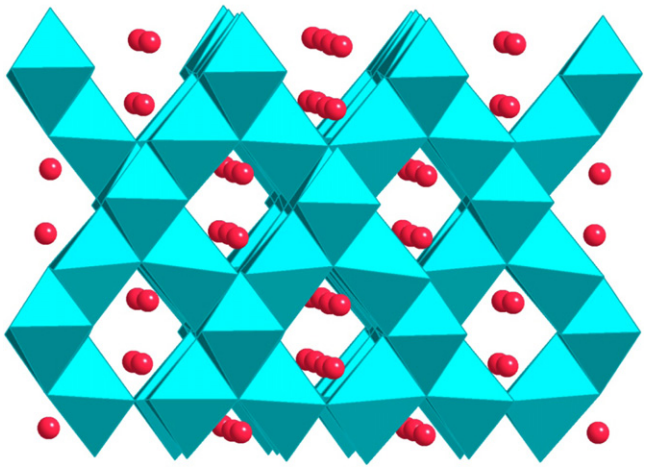

Fig. 8. Crystal structure of spinel LiM_2O_4 (blue: transition metal ions; red: Li ions). (For interpretation of the references to color in this figure legend, the reader is referred to the web version of the article.)

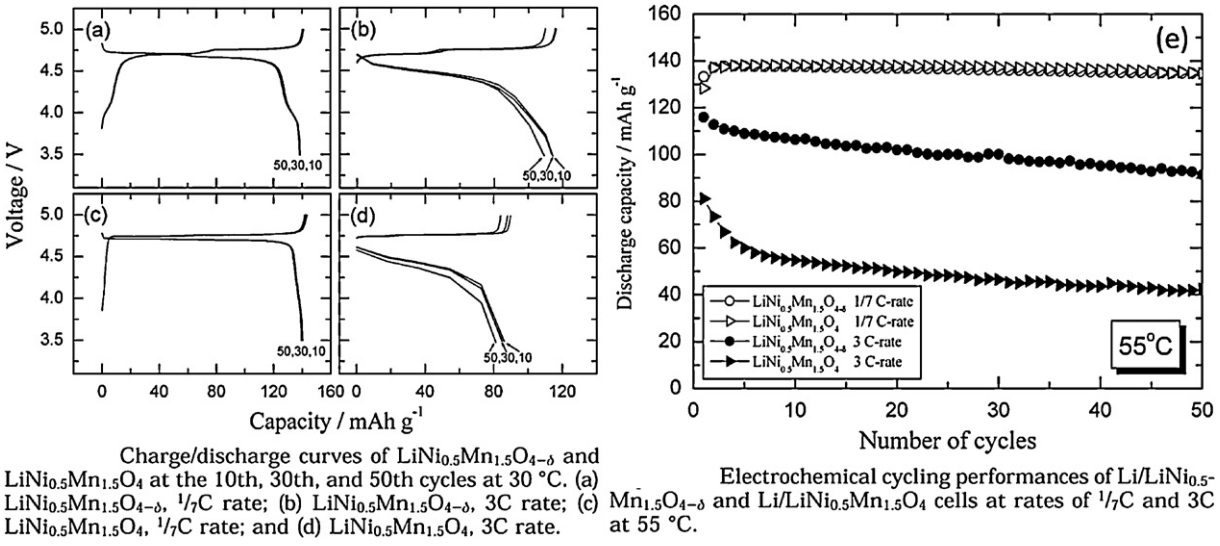

Charge/discharge curves of $LiNi_{0.5}Mn_{1.5}O_{4-\delta}$ and $LiNi_{0.5}Mn_{1.5}O_4$ at the 10th, 30th, and 50th cycles at 30 °C. (a) $LiNi_{0.5}Mn_{1.5}O_{4-\delta}$, 1/7C rate; (b) $LiNi_{0.5}Mn_{1.5}O_{4-\delta}$, 3C rate; (c) $LiNi_{0.5}Mn_{1.5}O_4$, 1/7C rate; and (d) $LiNi_{0.5}Mn_{1.5}O_4$, 3C rate.

Electrochemical cycling performances of Li/$LiNi_{0.5}Mn_{1.5}O_{4-\delta}$ and Li/$LiNi_{0.5}Mn_{1.5}O_4$ cells at rates of 1/7C and 3C at 55 °C.

Fig. 9. Performance of high voltage spinel $LiNi_{0.5}Mn_{1.5}O_4$ [71].

~4.7 V for $LiNi_{0.5}Mn_{1.5}O_4$, although in $LiNi_{0.5}Mn_{1.5}O_{4-x}$, a small voltage step appears at half lithium concentration. The theoretical capacity of $LiNi_{0.5}Mn_{1.5}O_4$ is calculated as 147 mAh/g, and more than 140 mAh/g reversible capacity can be obtained experimentally. With most of the Mn ions keeping Mn^{4+} unchanged during cycling, both ordered and disordered $LiNi_{0.5}Mn_{1.5}O_4$ exhibit good cycling performance for lower rate capability that there is little capacity fading after 50 cycles in room temperature (Fig. 9(a) and (c)) and elevated temperature (Fig. 9(e)). However, their rate capabilities still need to be improved. The disordered $LiNi_{0.5}Mn_{1.5}O_{4-x}$ shows better rate capability than ordered $LiNi_{0.5}Mn_{1.5}O_4$ for the material electronic conductivity is enhanced with the small amount of Mn^{3+} ions. The ionic conductivity is regarded as another rate-limiting factor. The Li diffusion coefficient of $LiNi_{0.5}Mn_{1.5}O_4$ was reported to in a wide range between 10^{-10} cm^2/s and 10^{-16} cm^2/s depending on different compositions and material morphologies [82–84].

As a further optimization approach, doping small amount of metal ions into $LiNi_{0.5}Mn_{1.5}O_4$ forming "bi-doped" spinel has been widely used, and certain properties of $LiNi_{0.5}Mn_{1.5}O_4$ can be further improved. A recent review paper by Yi et al. [85] has summarized the effect of different doping ions including both cation substitution and anion substitution. By doping other transition metal ions such as Fe, Cr, and Ti into ordered $LiNi_{0.5}Mn_{1.5}O_4$, the impurity phases may be limited and the cation disorder could be enhanced [86–90]. It was also reported that dopant such as Co and Cu may enhance the material electronic conductivity and/or lithium diffusion coefficient [91,92]. These enhancements therefore could further improve the material cycling performance and rate capability (Fig. 10 [92]). The doped bivalence metal ions such as Cumay also shift the 4.7 V plateau to even higher voltage therefore could further improve the energy density. However, for most of the dopants, the high voltage capacity is shortened and the overall reversible capacity is reduced. It was reported [86,92,93] that some doped ions such as Fe, Cu, Al, and Mg tend to occupy the tetrahedral sites and become inactive ions, not only reducing the capacity but also blocking the lithium diffusion pathways, therefore may impose a negative effect to the material performances.

Apart from chemistry modification, size minimization is also reported as an effective approach to improve the material rate capability. Highly crystalline $LiNi_{0.5}Mn_{1.5}O_4$ nano-sized particles can be successfully synthesized through different methods [79,94,95]. It was shown that the bulk properties of nano-sized particles are generally the same compared to micro-sized particles, although their surface areas increase causing increasing surface reactions. However, the small size shortened the Li diffusion length inside the active materials thus largely enhanced the material ionic conductivity. The rate capability of the nano-sized $LiNi_{0.5}Mn_{1.5}O_4$ therefore is highly improved as an overall effect [95,96]. It is important to point out the volumetric energy density (Wh/L) suffers from the size minimization greatly as most of the nano-sized materials do not have the optimized packing scheme yet.

In summary, the high voltage spinel material is promising due to its high energy density, perfect structural stability and good cycling performance under certain material modifications. The high voltage, however, is out of the voltage window of the current electrolyte, therefore causes the electrolyte decomposition and the formation of unstable SEI on composite cathode side during cycling. It is important to point out that the reversible capacity of this material is currently limited to 0.5 Li per MO_2 formula, which although is similar to the practical capacity of $LiCoO_2$, still is significantly lower comparing to the lithium nickel manganese layered compounds.

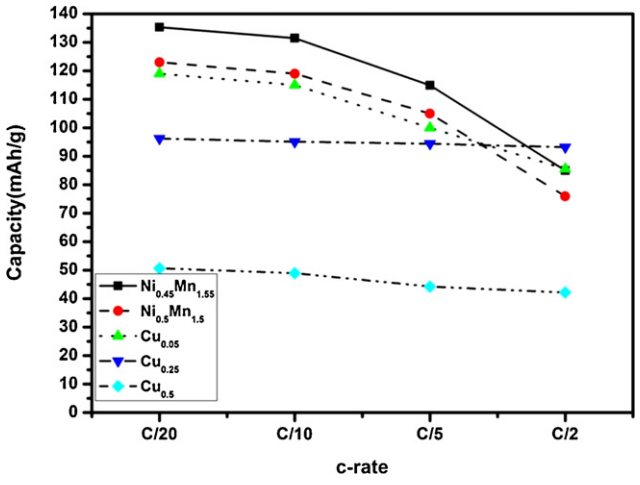

Fig. 10. Rate performance of rate capability of $LiNi_xCu_yMn_{2-x-y}O_4$ [92].

4. Olivine compounds $LiMPO_4$

Despite the early works back in 1980s [97,98], intensive studies on polyanion materials have not been conducted until recent fifteen years. These materials are receiving growing attentions because of the inherent stability of the polyanion group, which can delay or minimize the oxygen loss happening in traditional layer and spinel oxides.

Among all polyanion materials, olivine $LiFePO_4$ attracts the most interests due to its excellent electrochemical properties, as well as its low cost, non-toxicity, excellent thermal stability and environment friendliness. It was first found by Goodenough and coworkers in 1997 [99,100]. The structure of $LiFePO_4$ is shown in Fig. 11. It contains slightly distorted *hcp* anion oxygen arrays with half of the octahedral sites occupied by Fe and one eighth by Li. The LiO_6 octahedra are edge-shared while the FeO_6 octahedra are corner-shared. Both of the LiO_6 and FeO_6 run parallel to the *c* axis and they alternate in the *b* direction. The *a*–*c* planes containing the Li atoms are bridged by PO_4 tetrahedral. Three different paths of Li diffusion were proposed [101,102] and computational studies suggested that the one along *b* axis is much more favored than other paths across the channels [101,102]. In addition, in 2008 Yamada et al. further confirmed from experiments that the Li ion diffusion path along the (0 1 0) is a curved one dimension chain

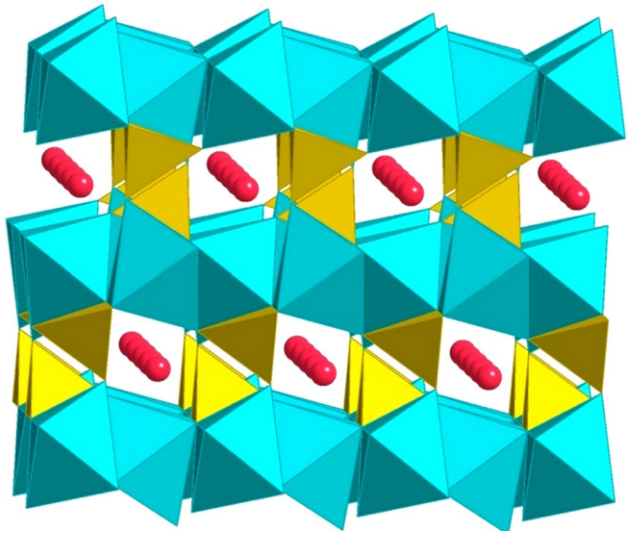

Fig. 11. Crystal structure of olivine $LiMPO_4$ (blue: transition metal ions; yellow: P ions; red Li ions). (For interpretation of the references to color in this figure legend, the reader is referred to the web version of the article.)

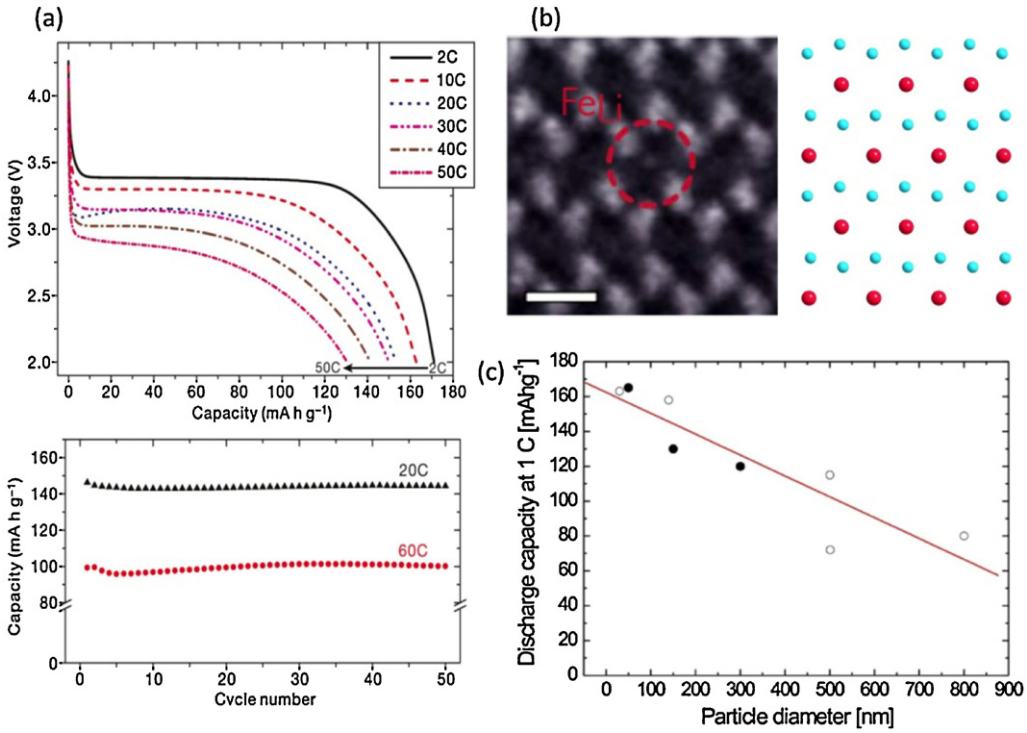

Fig. 12. Performance of olivine $LiFePO_4$: (a) after coating [118], (b) left: anti-site defect visualization under STEM [122], and right: atomic view of *b* axis (c) size dependence [123].

from high temperature powder neutron diffraction and the maximum entropy method [103]. Although the material shows excellent cycling performance, the main drawbacks of this material lie on its low energy density limited by the voltage, and its poor rate capability which is limited by the 1D ionic and poor intrinsic electronic conductivity. Different experimental approaches have been proposed to solve the problems: low voltage of the Fe^{3+}/Fe^{2+} redox couple can be overcome by applying other transition metal (TM) redox, such as Co, Mn, and Ni; three main different approaches have been proposed to improve the conductivity successfully, including: (1) surface modifications, i.e. coating the particles with a conductive film; (2) size modifications; (3) doping either Li or Fe sites with other metal ions.

Olivine structure can also be formed with transition metal ions other than Fe, such as Mn, Co and Ni. According to different active redox couples, the voltage is 4.1 V for $LiMnPO_4$ [99,104], 4.8 V for $LiCoPO_4$ [105] and 5.1 V for $LiNiPO_4$ [106]. Because of the limited voltage window of the current electrolyte, intensive research work have been done on $LiMnPO_4$ and doping $LiFePO_4$ with Mn, Co or Ni in Fe site (so-called divalent doping) [101,102,104,105,107–114] to get an optimal voltage as well as an enhancement in the performance. It has also been reported that substitution percentage can reach from 0% to 100% for Mn, Co, Ni and Mg dopants, while for Zn and Ca only partial substitution can be achieved [115].

Surface modifications with good electron conductor are believed to improve the electronic conductivity of the material, thus increase the rate capability. Conductive carbon is one of the popular coating materials that were proved to be effective. It was firstly shown by Armand et al. that by coating $LiFePO_4$ with a conductive carbon layer, more than 90% of theoretical capacity can be achieved at 80 °C in a polymer electrolyte cell [116]. Later, Nazar et al. found that by making $LiFePO_4$/C composite electrode, 90% of the theoretical capacity can be achieved at *C*/2 rate at room temperate, with good rate capability and stability [117]. In addition, surface modifications with other materials can also enhance the Li ion conductivity of the material. In 2009, Kang et al. proposed that Li ion conductivity at the surface between active material and electrolyte is the rate limiting step compared to the bulk with nanoscale particle size because of the anisotropic properties of the material. They modified the surface with glass lithium phosphate phase, which has high ionic conductivity. Excellent rate capability was achieved after the modification, as shown in Fig. 12(a) [118]. Capacity as high as 130 mAh/g at 50*C* is achieved and there is no fading even at 60*C* after 50 cycles.

Another approach is to minimize the particle size so as to shorten the Li ion diffusion length in the solid state as well as decrease the anti-site defect to increase the Li ion conductivity. Because of the one dimensional Li diffusion pathway in $LiFePO_4$, a single immobile defect would block the long way diffusion along the *b* axis. In the ideal ordered olivine structure, all Li reside in M1 site while all Fe are in M2 site. However, disorder, which is also called anti-site defect, is very common in LFP. Amin et al. [119] observed ~2.5 to 3% anti site defects, and in hydrothermally synthesized samples, up to ~7 to 8% anti site defects was observed [120]. The anti-site defect can be visualized under STEM [121,122], as shown in Fig. 12(b) [122]. Much effort has been taken to reduce the anti-site defect in the past few years. Chung et al. [121] reported that by a small amount of doping, the iron in the Li site can be controlled to aggregate together instead of randomly distribution, blocking fewer lithium channels. Later, it was shown by Lee et al. [122] that the segregation of Fe in Li site can be optimized by growth and/or annealing temperature. Gaberscek et al. reviewed nine papers by different research groups with different synthesis methods resulting in different particle sizes [123]. They concluded the capacity decreases linearly with the increase of particle size, shown in Fig. 12(c). Later work by Malik et al. reported that reducing particle size can help diminish the blocked capacity and nano-sized LFP is more tolerant to anti-site defects [124]. There are also studies on the air exposure effects on LFP/C nanocomposite [125,126], that the side reactions introduced by reducing size could be minimized by avoiding contact with oxidative moisture.

Doping both M1 site and M2 site has been studied over the past ten years. Besides divalent doping, aliovalent doping have been under debate [102,127–132] over the past ten years; recently the

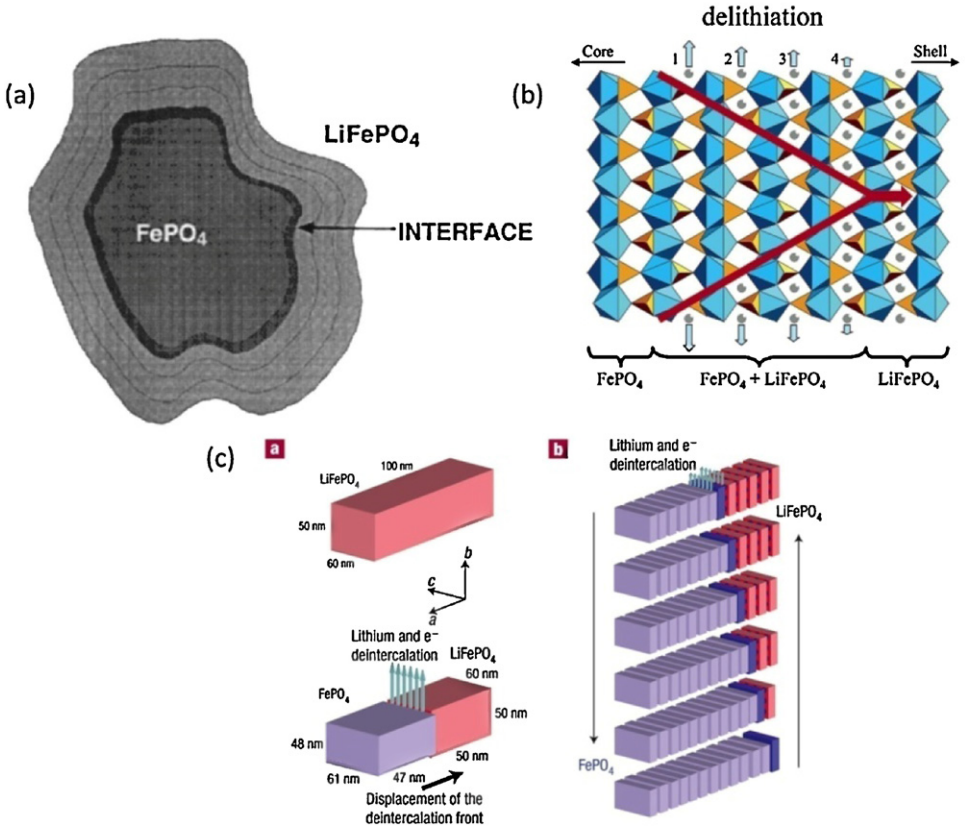

Fig. 13. Two phase mechanism of $LiFePO_4$: (a) classic shrinking core model [99], (b) anisotropic shrinking core model [137], and (c) domino-cascade model [138].

in lattice doping with Al^{3+}, Zr^{4+} and Nb^{5+} were clearly demonstrated by Meethong et al. [133]. As high as 12% (in atomic percentage) Zr was obtained. It is believed that the aliovalent doping can reduce the lithium miscibility gap as well as increase the phase transformation kinetics.

Besides property optimization, fundamental studies on olivine materials are also intensive due to its size dependent phase stabilities observed. For bulk $LiFePO_4$, its voltage profile is a plateau around 3.45 V vs. Li+/Li, which indicates a two-phase lithiation/delithiation process according to Gibbs phase rule. Yamada et al. [134] observed a room temperature miscibility gap between $Li_{0.05}FePO_4$ and $Li_{0.89}FePO_4$. Furthermore, Delacourt et al. [135] showed the experimental evidence of a temperature driven Li_xFePO_4 ($0 \leq x \leq 1$) solid solution at 450 °C, and two metastable phases $Li_{0.75}FePO_4$ and $Li_{0.5}FePO_4$ at room temperature in contrast to the well-believed two phase nature of the system. In addition, there is lots of debate in the community regarding whether this two phase process occurring is advantageous in terms of kinetics, conductivity as well as structural stability. Several studies on the two-phase mechanism have been carried out. It was first brought out by Padhi et al. [99] that the it follows the shrinking core model, shown in Fig. 13(a). They believed that with Li insertion, the interface area will shrink and the reaction will be diffusion limiting after reaching a critical surface area. It is vice versa for the delithiation process. However, Chen et al. [136] carried out TEM studies in 2006, which identified in single crystallites, there are intermediate zones between lithiated and delithiated phases. The shrinking core model cannot describe individual crystallites. Later the same year, Laffont et al. [137] conducted EELS study and confirmed that the classical shrinking core model cannot describe the mechanism due to the anisotropic lithium diffusion. They showed that there is no solid solution at the interface and the delithiation part is shown in Fig. 13(b). In 2008, Delmas et al. [138] proposed another delithiation mechanism using their domino-cascade model, as depicted in Fig. 13(c). The intercalation and deintercalation processes are explained to be a wave moving through the whole crystal along *a* axis due to minimizing the elastic energy caused by structural strains happening at the interface. This interface zone between the two phases provide good Li ion and electron conductivity. This domino-cascade model was further confirmed by Brunetti et al. [139] using precession electron diffraction technique. However, controversy still exists on the domino-cascade model [139].

In summary, olivine $LiFePO_4$ has a lower voltage and similar gravimetric energy density compared to $LiCoO_2$. However, its low cost, long life and environmental friendliness provide this material with high potentials to be the next generation of commercialized cathode materials. By (partially) substituting Fe with other transition metal ions such as Mn, Co or Ni, the voltage can be significantly improved. However, the intrinsic low conductivity of this series of materials is still the key problem because the size reduction and carbon coating increases the synthesis cost drastically.

5. Silicate compounds Li_2MSiO_4

Silicate material is relatively new to intercalation material. The potential for the extraction of two Li ions per unit formula in silicate materials first attracted a pioneer researcher Anton Nytén. In 2005, he investigated Li_2FeSiO_4 as the first material in the silicate family [140]. The structure of Li_2MSiO_4 is demonstrated in Fig. 14. The transition metal and silicate tetrahedra with corner sharing form a layered structure in which a 2-D zigzagging diffusion pathway is available for Li ion to intercalate and diffuse. Silicate materials can deliver a theoretical capacity up to 166 mAh/g for the extraction of one Li ion and 333 mAh/g when two Li ions

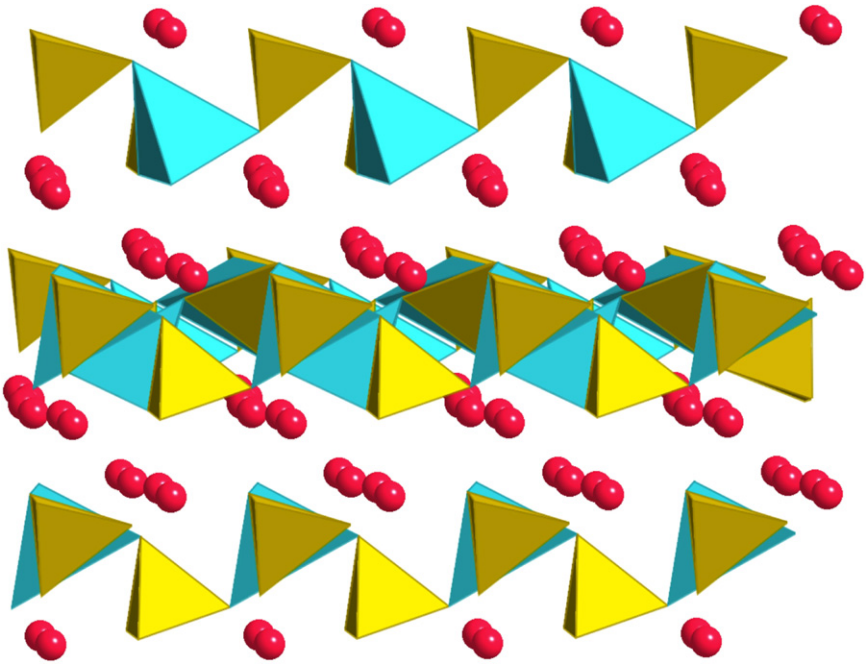

Fig. 14. Crystal structure of lithium intercalated silicates Li_2MSiO_4 (blue: transition metal ions; yellow: Si ions; red: Li ions). (For interpretation of the references to color in this figure legend, the reader is referred to the web version of the article.)

are extracted. Currently, the Fe, Mn, and the solid solution (e.g. $Li_2Mn_{0.5}Fe_{0.5}SiO_4$) versions of Li_2MSiO_4 have been synthesized via various synthesis routes such as hydrothermal, microwave-solvothermal, modified sol–gel, and solution [140–143]; however, the successful synthesis of the Ni version has eluded experimentalists so far.

Li_2FeSiO_4 was the first of the silicate family to be synthesized and was characterized by Nytén et al. in 2005 [140]. It was hypothesized that with carbon coating and nano particle size, the intrinsic low conductivity of silicate materials could be overcome. Li_2FeSiO_4 was synthesized using Li_2SiO_3 and $FeC_2O_4{\cdot}2H_2O$ mixed with carbon gel by the polymerization of the resorcinol–formaldehyde system [144,145]. Although the theoretical capacity of Li_2FeSiO_4 is two Li ions per formula unit (~333 mAh/g), it only delivered an initial charge capacity of 165 mAh/g and eventually stabilized around 140 mAh/g, indicating that less than one Li^+ ion per formula unit was extracted effectively. The synthesized material contained a mostly pure phase of Li_2FeSiO_4 with a space group of $Pmn2_1$ and parameters of $a = 6.2661(5)$ Å, $b = 5.3295(5)$ Å, and $c = 5.0148(4)$ Å. SEM demonstrated an average particle size of about 150 nm, and this particle size can be partially attributed to extended grinding. The electrochemical performance testing was conducted at elevated temperature of 60 °C with a $C/16$ current density rate. Cyclic voltammogram showed an oxidation peak shift from 3.1 to 2.8 V vs. Li/Li^+, suggesting a possible phase transformation within the Li_2FeSiO_4 structure. This phase transformation did not significantly affect lithium diffusion as the reversible capacity was stable at 140 mAh/g. Subsequently, this structure stability was also observed in the microwave-solvothermal synthesis of Li_2FeSiO_4 by Muraliganth et al. in 2010 [143]. Microwave-solvothermal synthesis method created a similar structure with same characteristics such as oxidation peak shift, while the particle sizes are different. Using this method, Muraliganthet al. were able to produce carbon-coated nanoparticles of approximately 20 nm. The decrease in particle size also inherently decreased the lithium ion diffusion path length. The reversible capacity greatly benefited from the improved morphology and was able to achieve 150 mAh/g at 25 °C and 200 mAh/g at 55 °C (Fig. 15) [143]. While only achieving the extraction of one lithium ion per unit formula, Li_2FeSiO_4 has been shown to possess exceptional structural stability.

Li_2MnSiO_4 was first synthesized via a modified Pechini sol–gel synthesis route by Dominko et al. in 2005. However, they did not succeed in the synthesis of Li_2MnSiO_4 via the hydrothermal synthesis route [141]. Lithium acetate dihyrate, manganese (II) acetate tetrahydrate and SiO_2 were prepared in two separate solutions and combined to form sol. The phase of Li_2MnSiO_4 was quite pure with little impurities including MnO and Li_2SiO_3, and XRD profiling revealed a $Pmn2_1$ space group with parameters of $a = 6.3109(9)$ Å, $b = 5.3800(9)$ Å, and $c = 4.9662(8)$ Å. Extensive Rietveld refinements showed that an ordered model did not match up with the XRD data. Hence, a disorder model was proposed with Li and Mn site exchanges and partial migration of Li, Mn, and Si to alternate tetrahedral sites being the two main disorder effects. This disordering could have worsened the amorphization of Li_2MnSiO_4 material during cycling. The sol–gel synthesis nature of the material did not provide the cathode material with any carbon nano-coating. This lack of conductivity manifested itself in terms of poor cycling and capacity retention of the material. On the first cycle only about 0.6 Li ions per formula unit were extracted, and this capacity rapidly faded to 0.3 reversibly exchanged lithium to within 5 cycles. A side note of this low capacity is the low cut off voltage chosen by the author to reduce effects of electrolyte degradation, which also lowered the effective lithium extraction.

Later experiments attempted to resolve and characterize the apparent rapid capacity fade of Li_2MnSiO_4 and the associated structural instability. Li et al. in 2007 synthesized carbon coated Li_2MnSiO_4 material via precipitation in solution route [146]. XRD refinement showed a similar cell parameter profile of $a = 6.308(3)$ Å, $b = 5.377(7)$ Å, and $c = 4.988(9)$ Å. The carbon coating drastically improved the electrochemical performance of Li_2MnSiO_4 to 209 mAh/g reversible capacity on the first charge; however, structural instability caused the capacity to fade to 140 mAh/g after 10 cycles. In situ characterization of the cathode material via XRD confirmed the structural instability by showing

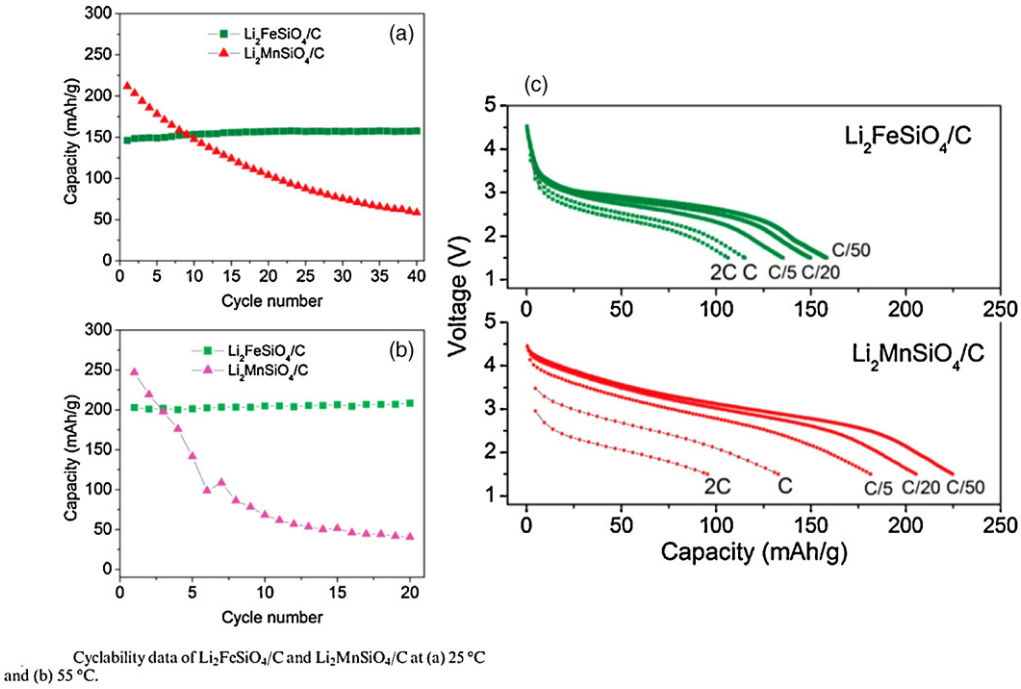

Cyclability data of Li_2FeSiO_4/C and Li_2MnSiO_4/C at (a) 25 °C and (b) 55 °C.

Fig. 15. (a) Cycling, (b) temperature, and (c) rate performance of Li_2MSiO_4 (M = Fe, Mn) [143].

the gradual amorphization of Li_2MnSiO_4 during the removal of Li ions in charging. The microwave solvothermal method was also used by Muraliganth et al. to synthesize Li_2MnSiO_4 [143]. The electrochemical properties were similar to the data presented by Li, and Muraliganth believes that the poor cycling retention of Li_2MnSiO_4 is mainly due to the Jahn–Teller distortion of Mn^{3+} and the structural instability it causes. Hence, Li_2MnSiO_4 still remains the high potential but troublesome member of the silicate family.

In 2006, Gong et al. also obtained the solid-state solution of $Li_2Mn_xFe_{1-x}SiO_4$ by a solution route [142]. Out of these materials created, the electrochemical tests of Li_2MnSiO_4 and $Li_2Mn_xFe_{1-x}SiO_4$ showed more than one Li ion per formula unit have been released based on the capacity obtained, although the possibilities cannot be excluded that the apparent capacity may be attributed to other side reactions. For $Li_2Mn_xFe_{1-x}SiO_4$, the solid-state solution achieved the highest initial charge capacity of 214 mAh/g when the ratio of Mn to Fe was 1:1,while the one with pure Fe and with 90% Mn can only achieve 140–150 mAh/g for first charge. However, the addition of Fe(II) into the Li_2MnSiO_4 structure did not prevent structural instabilities due to Mn oxidation since the cycling decay remained significant. The solid solution of different materials could give rise to a hybrid of material with more stable cycling and better capacity in the new silicate field.

While the search for new synthesis methods and optimization continue, silicate materials have shown certain promising properties in the field of intercalation materials. Li_2FeSiO_4 is capable of achieving 150–160 mAh/g at room temperature with great cycling retention, and performs even better at elevated

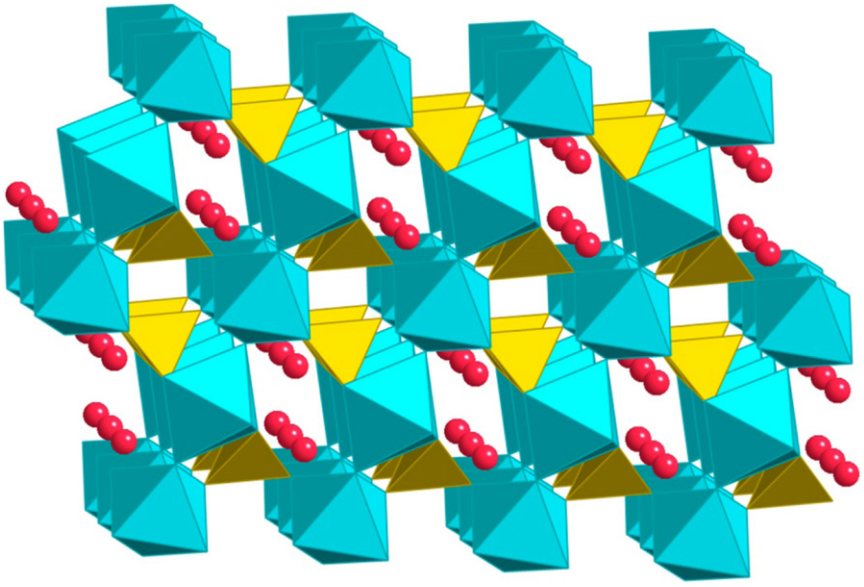

Fig. 16. Crystal structure of tavoriteLiMPO_4F (blue: transition metal ions; yellow: P ions; red: Li ions). (For interpretation of the references to color in this figure legend, the reader is referred to the web version of the article.)

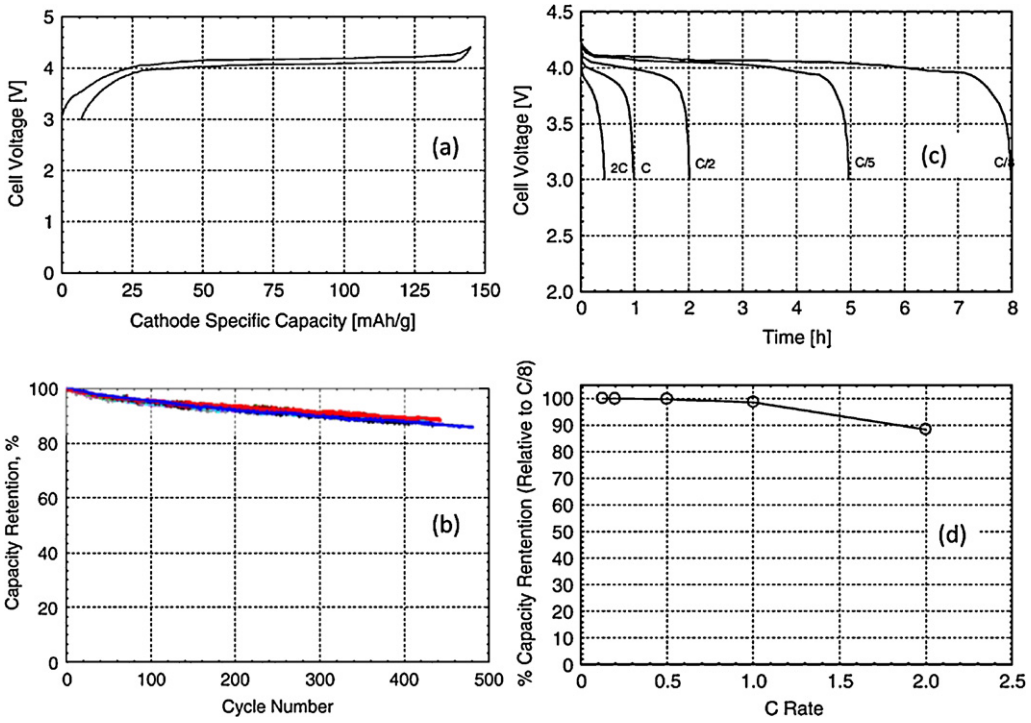

Fig. 17. (a) First cycle voltage profile of $LiVPO_4F$, (b) cycling performance of $LiVPO_4F$, and (c) and (d) rate performance of $LiVPO_4F$ [147].

temperatures of 55 °C. Li_2MnSiO_4, on the other hand, suffers from significant structural instability that causes fast capacity fading, although its initial capacity around 200 mAh/g is higher than Li_2FeSiO_4. More research is needed on the characterization of these materials to understand the nature of phase changes during cycling so that cycling performance of Li_2MnSiO_4 can be improved.

6. Tavorite compounds $LiMPO_4F$

Tavorite is a derivative class of the olivine structure and shares many of the characteristics with the olivine series. The crystal structure of $LiMPO_4F$ is shown in Fig. 16, where lithium ions are surrounded by transition metal octahedra and phosphate tetrahedra. Tavorites have good thermal stability due to the strength of the phosphorus and oxygen bonds, but suffer from low energy density. The introduction of fluorine into the structure opens up the 1D ionic pathways to multidimensional pathways for Li diffusion [147].

$LiVPO_4F$ represents the typical tavorite material, with crystal structure similar to the naturally occurring mineral amblygonite $LiAlPO_4F$. The structure of $LiVPO_4F$ is described as phosphate tetrahedra corner sharing with vanadium octahedra. Each vanadium atom is bonded with four oxygen atoms and two fluorine atoms, and lithium exists in two different sites within the structure. A carbothermal reduction method was used to synthesize $LiVPO_4F$ with VPO_4 and LiF as precursors [148,149]. Fig. 17 showed the electrochemical testing results of $LiVPO_4F$ [147]. A discharge capacity around 140 mAh/g is delivered with average discharge voltage of 4.05 V. After 400 cycles at $C/2$ rate, 90% of the initial capacity remained. This excellent cycling performance suggests great structural stability with no phase transformation. $LiVPO_4F$ also exhibits good rate capability, retaining 90% of the capacity when charged at $2C$ rate. Multidimensional diffusion pathways for Li ion transport in tavorite materials are the distinguishing characteristics from olivine materials. As expected from structural stability, $LiVPO_4F$ shows superior thermal stability up to 175 °C. $LiVPO_4F$ represents a new class of material that has great capacity retention, rate capability, and thermal stability.

$LiFePO_4F$ is also being studied closely in the tavorite class. Different from most of other intercalation materials, $LiFePO_4F$ starts in the charged state and is then subsequently discharged to form Li_2FePO_4F. Particle size of about 1 μm has been reported for solid state synthesis with $FePO_4$ and LiF [150]. Since tavorites have high ionic conductivity due to robust diffusion pathways, nanoparticle size is not required for the material to be

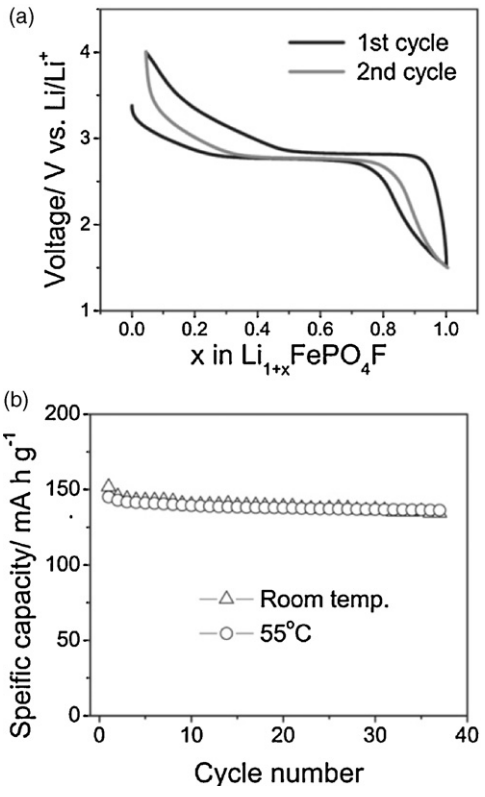

Fig. 18. Cycling and temperature performance of Li_2FePO_4F [150].

electrochemically active. During $LiFePO_4F$ synthesis, the absence of hydroxyl groups is crucial for electrochemical reversibility. The mechanism of hydroxyl group interactions is not well characterized and could be due to major phase changes during cycling. The complete extraction of Li from $LiFePO_4F$ is limited by the high redox potential of Fe(III) to Fe(IV), hence $LiFePO_4F$ has been limited to the effective intercalation of one Li^+ ion per unit formula. Electrochemical testing has shown excellent capacity retention of about 150 mAh/g over 40 cycles even at elevated temperature (Fig. 18 [150]). The spacious diffusion tunnels provided by the tavorite structure provide the material with minimal interactions between the Li^+ ions and the residing structure.

In summary, tavorites have emerged as a good alternative to the olivine class of materials due to exceptional ionic conductivity, thermal stability, and capacity retention. However, its energy density is still limited by the amount of lithium available for intercalation and much of the details of phase transformation are still yet to be fully characterized.

7. Borate compounds $LiMBO_3$

Borates $LiMBO_3$ have received much attention because of its lightest polyanion group, BO_3, which ensures higher theoretical energy density than other polyanion cathode materials. Legagneur et al. first reported the electrochemical properties of $LiMBO_3$ (M = Mn, Fe, Co), which can only (de)intercalate 0.04Li per formula, i.e. 9 mAh/g, at a rate of *C*/250 (the theoretical capacity is 220 mAh/g) [151]. The structure of $LiFeBO_3$ is shown in Fig. 19. The three dimensional $FeBO_3$ framework is built from FeO_5 bipyramids and BO_3 trigonal planar. The FeO_5 bipyramids share edges along $[\bar{1}\,0\,1]$ direction forming single chains, and the BO_3 are corner shared with three chains. Within this three dimensional framework, Li occupies two tetrahedral sites sharing an edge, which forms chains running along the [0 0 1] direction. It was later found by Dong et al. [152] that they can obtain 91.8 mAh/g for the initial discharge. They also applied carbon as a coating material as well as for making the $LiFeBO_3$/C composite, and higher discharge capacity values (158.3 mAh/g at 5 mA/g and 122.9 mAh/g at 50 mA/g) were obtained [153].

The full potential of this material was not optimized until 2010, by Yamada et al. [154], approaching a capacity of 200 mAh/g supported by both experimental and computational results. According to their opinions, surface poisoning by moisture in air is the main source of contamination happening in previous studies. With proper handling of the samples and electrodes, the theoretical capacity was almost achieved at *C*/20 rate, and more than 75% of the theoretical capacity was achieved at 2*C* rate, as shown in Fig. 20.

Besides $LiFeBO_3$, Mn based borates have been studied over the past two years as well [151,155,156]. $LiMnBO_3$ has two polymorphs, hexagonal [151,155] and monoclinic [156]. The hexagonal phase was claimed to have an initial discharge capacity of 75.5 mAh/g with a wide voltage window range, 1.0–4.8 V [155]. While for the monoclinic phase, electrochemical data was not shown until 2011 [156], a second discharge of 100 mAh/g with good retention over multiple cycles on carbon coated $LiMnBO_3$ was observed.

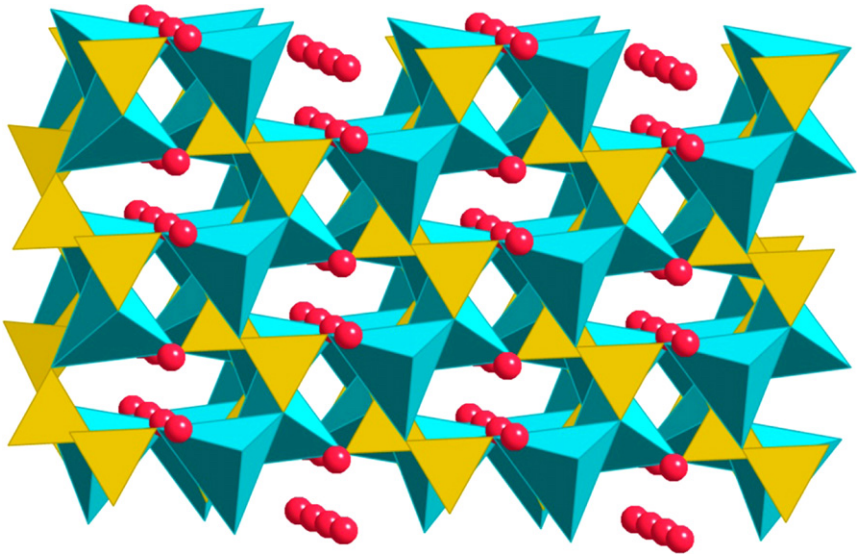

Fig. 19. structure of LiFeBO3 (green: transition metal ions; orange: B ions; red: Li ions). (For interpretation of the references to color in this figure legend, the reader is referred to the web version of the article.)

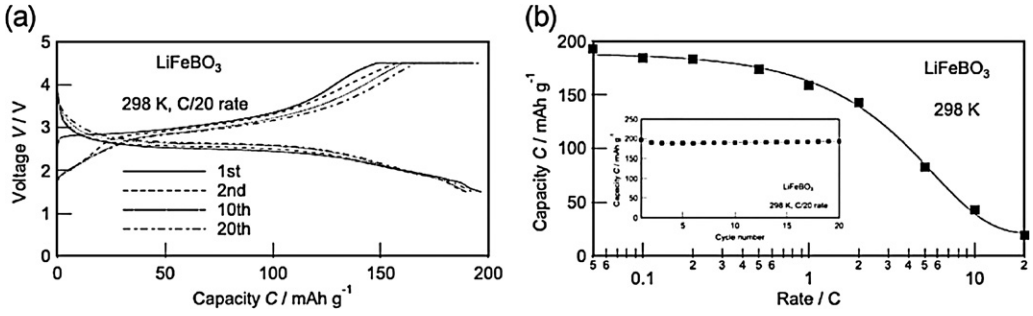

Fig. 20. $LiFeBO_3$ performance [154].

Borates being one of the newest generations of the Li intercalation materials, its performance is relatively poor comparing to other cathode materials. The recent studies have shown that the kinetic polarization and the moisture sensitivity should be the main limiting factors and much work is still needed to explore the optimized synthesize and operation conditions.

8. Conclusion

In this review we focus on recent progress made in cathode materials in lithium ion batteries, toward higher energy density, higher power density, longer cycle life and better safety characteristics. In six different materials chemistry families, we describe the crystal structures, the redox potentials, the ion mobilities, the possible phase transformation mechanisms and structural stability changes, and their relevance to the high-energy high-power low-cost electrochemical systems. Over the past decade, we have seen ample examples where a combination of virtual materials design/characterization and knowledge-guided experimentation have made significant impacts on changing the traditional trial-and-true way of materials design; many of them have accelerated the pace of development of new high energy high power density electrode materials for LIB. We also reviewed two important aspects of materials engineering modification for cathode materials in LIB: nano-structure synthesis and surface modification for each material chemistry. It is important to point out that the trend toward nano-structure electrode design must be balanced with careful consideration on the volumetric energy density. Most of the nano-structured materials have high porosities and low volumetric energy Wh/L values, the deployment of which will be limited in the energy storage applications where space is a prime concern. Surface modification can help improve electrochemical properties, though fundamental understanding still lags behind. It is also critical to use cost-effective and scalable synthesis methods to apply the surface modification. Very recently, high-throughput computational methods have been implemented and utilized to screen for new novel electrode materials [157–159]. In the near future we will see a paradigm shift on advanced materials discovery and optimization. Computational tools will be critically important to enable new electrode materials development and optimization, at the same time minimizing the traditional experimental trials.

Acknowledgement

The authors acknowledge the financial support from the National Science Foundation under grant number DMR 1057170.

References

[1] K. Mizushima, P.C. Jones, P.J. Wiseman, J.B. Goodenough, Materials Research Bulletin 15 (1980) 783–789.
[2] T. Ohzuku, A. Ueda, M. Nagayama, Y. Iwakoshi, H. Komori, Electrochimica Acta 38 (1993) 1159–1167.
[3] J.M. Tarascon, D. Guyomard, Electrochimica Acta 38 (1993) 1221–1231.
[4] Y.Y. Xia, M. Yoshio, Journal of the Electrochemical Society 143 (1996) 825–833.
[5] G. Ceder, Y.M. Chiang, D.R. Sadoway, M.K. Aydinol, Y.I. Jang, B. Huang, Nature 392 (1998) 694–696.
[6] J.M. Tarascon, M. Armand, Nature 414 (2001) 359–367.
[7] F. Croce, A.D. Epifanio, J. Hassoun, A. Deptula, T. Olczac, B. Scrosati, Electrochemical and Solid-State Letters 5 (2002) A47–A50.
[8] M.S. Whittingham, Chemical Reviews 104 (2004) 4271–4301.
[9] T. Ohzuku, Y. Makimura, Chemistry Letters (2001) 744–745.
[10] X.L. Meng, S.M. Dou, W.L. Wang, Journal of Power Sources 184 (2008) 489–493.
[11] K.S. Kang, Y.S. Meng, J. Breger, C.P. Grey, G. Ceder, Science 311 (2006) 977–980.
[12] W.S. Yoon, C.P. Grey, M. Balasubramanian, X.Q. Yang, J. McBreen, Chemistry of Materials 15 (2003) 3161–3169.
[13] A. Abdel-Ghany, K. Zaghib, F. Gendron, A. Mauger, C.M. Julien, Electrochimica Acta 52 (2007) 4092–4100.
[14] J. Breger, N. Dupre, P.J. Chupas, P.L. Lee, T. Proffen, J.B. Parise, C.P. Grey, Journal of the American Chemical Society 127 (2005) 7529–7537.
[15] Y.S. Meng, G. Ceder, C.P. Grey, W.S. Yoon, Y. Shao-Horn, Electrochemical and Solid-State Letters 7 (2004) A155–A158.
[16] A. Van der Ven, G. Ceder, Electrochemistry Communications 6 (2004) 1045–1050.
[17] Z.H. Lu, D.D. MacNeil, J.R. Dahn, Electrochemical and Solid-State Letters 4 (2001) A191–A194.
[18] W.S. Yoon, Y. Paik, X.Q. Yang, M. Balasubramanian, J. McBreen, C.P. Grey, Electrochemical and Solid-State Letters 5 (2002) A263–A266.
[19] J. Breger, Y.S. Meng, Y. Hinuma, S. Kumar, K. Kang, Y. Shao-Horn, G. Ceder, C.P. Grey, Chemistry of Materials 18 (2006) 4768–4781.
[20] N. Yabuuchi, S. Kumar, H.H. Li, Y.T. Kim, Y. Shao-Horn, Journal of the Electrochemical Society 154 (2007) A566–A578.
[21] N. Yabuuchi, Y.T. Kim, H.H. Li, Y. Shao-Horn, Chemistry of Materials 20 (2008) 4936–4951.
[22] Y. Hinuma, Y.S. Meng, K.S. Kang, G. Ceder, Chemistry of Materials 19 (2007) 1790–1800.
[23] M.S. Whittingham, Science 192 (1976) 1126–1127.
[24] T. Ohzuku, Y. Makimura, Chemistry Letters (2001) 642–643.
[25] N. Yabuuchi, T. Ohzuku, Journal of Power Sources 146 (2005) 636–639.
[26] K.M. Shaju, P.G. Bruce, Advanced Materials 18 (2006) 2330.
[27] M.H. Lee, Y. Kang, S.T. Myung, Y.K. Sun, Electrochimica Acta 50 (2004) 939–948.
[28] P.S. Whitfield, I.J. Davidson, L.M.D. Cranswick, I.P. Swainson, P.W. Stephens, Solid State Ionics 176 (2005) 463–471.
[29] N. Yabuuchi, Y. Koyama, N. Nakayama, T. Ohzuku, Journal of the Electrochemical Society 152 (2005) A1434–A1440.
[30] J.M. Kim, H.T. Chung, Electrochimica Acta 49 (2004) 937–944.
[31] D.C. Li, T. Muta, L.Q. Zhang, M. Yoshio, H. Noguchi, Journal of Power Sources 132 (2004) 150–155.
[32] J. Choi, A. Manthiram, Journal of the Electrochemical Society 152 (2005) A1714–A1718.
[33] Y. Koyama, I. Tanaka, H. Adachi, Y. Makimura, T. Ohzuku, Journal of Power Sources 119 (2003) 644–648.
[34] B.J. Hwang, Y.W. Tsai, D. Carlier, G. Ceder, Chemistry of Materials 15 (2003) 3676–3682.
[35] W.S. Yoon, C.P. Grey, M. Balasubramanian, X.Q. Yang, D.A. Fischer, J. McBreen, Electrochemical and Solid-State Letters 7 (2004) A53–A55.
[36] A. Manthiram, J. Choi, Journal of Power Sources 159 (2006) 249–253.
[37] Z. Li, N.A. Chernova, M. Roppolo, S. Upreti, C. Petersburg, F.M. Alamgir, M.S. Whittingham, Journal of the Electrochemical Society 158 (2011) A516–A522.
[38] Z.H. Lu, L.Y. Beaulieu, R.A. Donaberger, C.L. Thomas, J.R. Dahn, Journal of the Electrochemical Society 149 (2002) A778–A791.
[39] W.S. Yoon, S. Iannopollo, C.P. Grey, D. Carlier, J. Gorman, J. Reed, G. Ceder, Electrochemical and Solid-State Letters 7 (2004) A167–A171.
[40] Y.S. Meng, G. Ceder, C.P. Grey, W.S. Yoon, M. Jiang, J. Breger, Y. Shao-Horn, Chemistry of Materials 17 (2005) 2386–2394.
[41] J. Breger, M. Jiang, N. Dupre, Y.S. Meng, Y. Shao-Horn, G. Ceder, C.P. Grey, Journal of Solid State Chemistry 178 (2005) 2575–2585.
[42] C.H. Lei, J. Bareno, J.G. Wen, I. Petrov, S.H. Kang, D.P. Abraham, Journal of Power Sources 178 (2008) 422–433.
[43] C.R. Fell, K.J. Carroll, M.F. Chi, Y.S. Meng, Journal of the Electrochemical Society 157 (2010) A1202–A1211.
[44] B. Xu, C.R. Fell, M.F. Chi, Y.S. Meng, Energy & Environmental Science 4 (2011) 2223–2233.
[45] A. van Bommel, J.R. Dahn, Electrochemical and Solid-State Letters 13 (2010) A62–A64.
[46] M.M. Thackeray, S.H. Kang, C.S. Johnson, J.T. Vaughey, R. Benedek, S.A. Hackney, Journal of Materials Chemistry 17 (2007) 3112–3125.
[47] A.R. Armstrong, M. Holzapfel, P. Novak, C.S. Johnson, S.H. Kang, M.M. Thackeray, P.G. Bruce, Journal of the American Chemical Society 128 (2006) 8694–8698.
[48] Z.H. Lu, J.R. Dahn, Journal of the Electrochemical Society 149 (2002) A815–A822.
[49] M. Jiang, B. Key, Y.S. Meng, C.P. Grey, Chemistry of Materials 21 (2009) 2733–2745.
[50] A.D. Robertson, P.G. Bruce, Electrochemical and Solid-State Letters 7 (2004) A294–A298.
[51] C.P. Grey, W.S. Yoon, J. Reed, G. Ceder, Electrochemical and Solid-State Letters 7 (2004) A290–A293.
[52] J. Liu, A. Manthiram, Journal of Materials Chemistry 20 (2010) 3961–3967.
[53] S.T. Myung, K. Izumi, S. Komaba, Y.K. Sun, H. Yashiro, N. Kumagai, Chemistry of Materials 17 (2005) 3695–3704.
[54] S.-T. Myung, K. Izumi, S. Komaba, H. Yashiro, H.J. Bang, Y.-K. Sun, N. Kumagai, Journal of Physical Chemistry C 111 (2007) 4061–4067.
[55] S.T. Myung, K.S. Lee, C.S. Yoon, Y.K. Sun, K. Amine, H. Yashiro, Journal of Physical Chemistry C 114 (2010) 4710–4718.
[56] B.C. Park, H.B. Kim, S.T. Myung, K. Amine, I. Belharouak, S.M. Lee, Y.K. Sun, Journal of Power Sources 178 (2008) 826–831.
[57] J. Cho, H. Kim, B. Park, Journal of the Electrochemical Society 151 (2004) A1707–A1711.
[58] Q.Y. Wang, J. Liu, A.V. Murugan, A. Manthiram, Journal of Materials Chemistry 19 (2009) 4965–4972.
[59] Y. Wu, A. Manthiram, Solid State Ionics 180 (2009) 50–56.
[60] Y.K. Sun, S.T. Myung, B.C. Park, J. Prakash, I. Belharouak, K. Amine, Nature Materials 8 (2009) 320–324.
[61] M.M. Thackeray, W.I.F. David, P.G. Bruce, J.B. Goodenough, Materials Research Bulletin 18 (1983) 461–472.
[62] J.B. Goodenough, M.M. Thackeray, W.I.F. David, P.G. Bruce, Revue de Chimie Minerale 21 (1984) 435–455.

[63] W.I.F. David, M.M. Thackeray, P.G. Bruce, J.B. Goodenough, Materials Research Bulletin 19 (1984) 99–106.
[64] D. Aurbach, M.D. Levi, K. Gamulski, B. Markovsky, G. Salitra, E. Levi, U. Heider, L. Heider, R. Oesten, Journal of Power Sources 81 (1999) 472–479.
[65] Y.Y. Xia, Y.H. Zhou, M. Yoshio, Journal of the Electrochemical Society 144 (1997) 2593–2600.
[66] Y.J. Shin, A. Manthiram, Journal of the Electrochemical Society 151 (2004) A204–A208.
[67] R.J. Gummow, A. Dekock, M.M. Thackeray, Solid State Ionics 69 (1994) 59–67.
[68] K.-S. Lee, S.-T. Myung, H.J. Bang, S. Chung, Y.-K. Sun, Electrochimica Acta 52 (2007) 5201–5206.
[69] Y.J. Lee, S.H. Park, C. Eng, J.B. Parise, C.P. Grey, Chemistry of Materials 14 (2002) 194–205.
[70] L. Hernan, J. Morales, L. Sanchez, J. Santos, Solid State Ionics 118 (1999) 179–185.
[71] J.H. Kim, S.T. Myung, C.S. Yoon, S.G. Kang, Y.K. Sun, Chemistry of Materials 16 (2004) 906–914.
[72] G.H. Li, H. Ikuta, T. Uchida, M. Wakihara, Journal of the Electrochemical Society 143 (1996) 178–182.
[73] J. Molenda, J. Marzec, K. Swierczek, W. Ojczyk, M. Ziemnicki, M. Molenda, M. Drozdek, R. Dziembaj, Solid State Ionics 171 (2004) 215–227.
[74] T. Ohzuku, S. Takeda, M. Iwanaga, Journal of Power Sources 81–82 (1999) 90–94.
[75] R. Singhal, S.R. Das, M.S. Tomar, O. Ovideo, S. Nieto, R.E. Melgarejo, R.S. Katiyar, Journal of Power Sources 164 (2007) 857–861.
[76] J. Tu, X.B. Zhao, D.G. Zhuang, G.S. Cao, T.J. Zhu, J.P. Tu, Physica B: Condensed Matter 382 (2006) 129–134.
[77] S.T. Yang, J.H. Jia, L. Ding, M.C. Zhang, Electrochimica Acta 48 (2003) 569–573.
[78] K. Takahashi, M. Saitoh, M. Sano, M. Fujita, K. Kifune, Journal of the Electrochemical Society 151 (2004) A173–A177.
[79] S.T. Myung, S. Komaba, N. Kumagai, H. Yashiro, H.T. Chung, T.H. Cho, Electrochimica Acta 47 (2002) 2543–2549.
[80] Q.M. Zhong, A. Bonakdarpour, M.J. Zhang, Y. Gao, J.R. Dahn, Journal of the Electrochemical Society 144 (1997) 205–213.
[81] J.H. Kim, S.T. Myung, Y.K. Sun, Electrochimica Acta 49 (2004) 219–227.
[82] M. Kunduraci, G.G. Amatucci, Electrochimica Acta 53 (2008) 4193–4199.
[83] H. Xia, Y.S. Meng, L. Lu, G. Ceder, Journal of the Electrochemical Society 154 (2007) A737–A743.
[84] J.S. Yang, J.J. Xu, Journal of the Electrochemical Society 153 (2006) A716–A723.
[85] T.F. Yi, Y. Xie, M.F. Ye, L.J. Jiang, R.S. Zhu, Y.R. Zhu, Ionics 17 (2011) 383–389.
[86] G.T.K. Fey, C.Z. Lu, T.P. Kumar, Journal of Power Sources 115 (2003) 332–345.
[87] T.A. Arunkumar, A. Manthiram, Electrochimica Acta 50 (2005) 5568–5572.
[88] M. Aklalouch, J.M. Amarilla, R.M. Rojas, I. Saadoune, J.M. Rojo, Journal of Power Sources 185 (2008) 501–511.
[89] D.C. Li, A. Ito, K. Kobayakawa, H. Noguchi, Y. Sato, Journal of Power Sources 161 (2006) 1241–1246.
[90] J. Liu, A. Manthiram, Journal of Physical Chemistry C 113 (2009) 15073–15079.
[91] A. Ito, D. Li, Y. Lee, K. Kobayakawa, Y. Sato, Journal of Power Sources 185 (2008) 1429–1433.
[92] M.C. Yang, B. Xu, J.H. Cheng, C.J. Pan, B.J. Hwang, Y.S. Meng, Chemistry of Materials 23 (2011) 2832–2841.
[93] Y. Ein-Eli, J.T. Vaughey, M.M. Thackeray, S. Mukerjee, X.Q. Yang, J. McBreen, Journal of the Electrochemical Society 146 (1999) 908–913.
[94] J.C. Arrebola, A. Caballero, M. Cruz, L. Hernan, J. Morales, E.R. Castellon, Advanced Functional Materials 16 (2006) 1904–1912.
[95] K.M. Shaju, P.G. Bruce, Dalton Transactions (2008) 5471–5475.
[96] Y. Talyosef, B. Markovsky, R. Lavi, G. Salitra, D. Aurbach, D. Kovacheva, M. Gorova, E. Zhecheva, R. Stoyanova, Journal of the Electrochemical Society 154 (2007) A682–A691.
[97] A. Manthiram, J.B. Goodenough, Journal of Power Sources 26 (1989) 403–408.
[98] C. Delmas, A. Nadiri, J.L. Soubeyroux, Solid State Ionics 28 (1988) 419–423.
[99] A.K. Padhi, Journal of the Electrochemical Society 144 (1997) 1188.
[100] A.K. Padhi, K.S. Nanjundaswamy, C. Masquelier, S. Okada, J.B. Goodenough, Journal of the Electrochemical Society 144 (1997) 1609–1613.
[101] D. Morgan, A. Van der Ven, G. Ceder, Electrochemical and Solid-State Letters 7 (2004) A30–A32.
[102] C.A.J. Fisher, V.M. Hart Prieto, M.S. Islam, Chemistry of Materials 20 (2008) 5907–5915.
[103] S.-i. Nishimura, G. Kobayashi, K. Ohoyama, R. Kanno, M. Yashima, A. Yamada, Nature Materials 7 (2008) 707–711.
[104] A. Yamada, S.C. Chung, Journal of the Electrochemical Society 148 (2001) A960–A967.
[105] J. Wolfenstine, J. Allen, Journal of Power Sources 136 (2004) 150–153.
[106] J. Wolfenstine, J. Allen, Journal of Power Sources 142 (2005) 389–390.
[107] D. Wang, H. Li, S. Shi, X. Huang, L. Chen, Electrochimica Acta 50 (2005) 2955–2958.
[108] T. Drezen, N.H. Kwon, P. Bowen, I. Teerlinck, M. Isono, I. Exnar, Journal of Power Sources 174 (2007) 949–953.
[109] G. Kobayashi, A. Yamada, S. Nishimura, R. Kanno, Y. Kobayashi, S. Seki, Y. Ohno, H. Miyashiro, Journal of Power Sources 189 (2009) 397–401.
[110] M. Kopec, A. Yamada, G. Kobayashi, S. Nishimura, R. Kanno, A. Mauger, F. Gendron, C.M. Julien, Journal of Power Sources 189 (2009) 1154–1163.
[111] A. Yamada, Y. Kudo, K.Y. Liu, Journal of the Electrochemical Society 148 (2001) A1153–A1158.
[112] A. Yamada, Y. Kudo, K.Y. Liu, Journal of the Electrochemical Society 148 (2001) A747–A754.
[113] A. Yamada, Y. Takei, H. Koizumi, N. Sonoyama, R. Kanno, Applied Physics Letters 87 (2005).
[114] A. Yamada, Y. Takei, H. Koizumi, N. Sonoyama, R. Kanno, K. Itoh, M. Yonemura, T. Kamiyama, Chemistry of Materials 18 (2006) 804–813.
[115] J. Chen, M.J. Vacchio, S. Wang, N. Chernova, P.Y. Zavalij, M.S. Whittingham, Solid State Ionics 178 (2008) 1676–1693.
[116] N. Ravet, Y. Chouinard, J.F. Magnan, S. Besner, M. Gauthier, M. Armand, Journal of Power Sources 97–8 (2001) 503–507.
[117] H. Huang, S.C. Yin, L.F. Nazar, Electrochemical and Solid-State Letters 4 (2001) A170–A172.
[118] B. Kang, G. Ceder, Nature 458 (2009) 190–193.
[119] R. Amin, P. Balaya, J. Maier, Electrochemical and Solid-State Letters 10 (2007) A13–A16.
[120] S.F. Yang, Y.N. Song, P.Y. Zavalij, M.S. Whittingham, Electrochemistry Communications 4 (2002) 239–244.
[121] S.-Y. Chung, S.-Y. Choi, T. Yamamoto, Y. Ikuhara, Angewandte Chemie International Edition 48 (2009) 543–546.
[122] J. Lee, W. Zhou, J.C. Idrobo, S.J. Pennycook, S.T. Pantelides, Physical Review Letters 107 (2011) 085507.
[123] M. Gaberscek, R. Dominko, J. Jamnik, Electrochemistry Communications 9 (2007) 2778–2783.
[124] R. Malik, D. Burch, M. Bazant, G. Ceder, Nano Letters 10 (2010) 4123–4127.
[125] J.F. Martin, M. Cuisinier, N. Dupre, A. Yamada, R. Kanno, D. Guyomard, Journal of Power Sources 196 (2011) 2155–2163.
[126] J.F. Martin, A. Yamada, G. Kobayashi, S.I. Nishimura, R. Kanno, D. Guyomard, N. Dupre, Electrochemical and Solid-State Letters 11 (2008) A12–A16.
[127] M.S. Islam, D.J. Driscoll, C.A.J. Fisher, P.R. Slater, Chemistry of Materials 17 (2005) 5085–5092.
[128] C. Delacourt, C. Wurm, L. Laffont, J.B. Leriche, C. Masquelier, Solid State Ionics 177 (2006) 333–341.
[129] B. Ellis, P. Subramanya Herle, Y.H. Rho, L.F. Nazar, R. Dunlap, L.K. Perry, D.H. Ryan, Faraday Discussions 134 (2007) 119.
[130] K. Zaghib, A. Mauger, J.B. Goodenough, F. Gendron, C.M. Julien, Chemistry of Materials 19 (2007) 3740–3747.
[131] R. Amin, C.T. Lin, J. Maier, Physical Chemistry Chemical Physics 10 (2008) 3519–3523.
[132] M. Wagemaker, B.L. Ellis, D. Luetzenkirchen-Hecht, F.M. Mulder, L.F. Nazar, Chemistry of Materials 20 (2008) 6313–6315.
[133] N. Meethong, Y.H. Kao, S.A. Speakman, Y.M. Chiang, Advanced Functional Materials 19 (2009) 1060–1070.
[134] A. Yamada, H. Koizumi, S.I. Nishimura, N. Sonoyama, R. Kanno, M. Yonemura, T. Nakamura, Y. Kobayashi, Nature Materials 5 (2006) 357–360.
[135] C. Delacourt, P. Poizot, J.M. Tarascon, C. Masquelier, Nature Materials 4 (2005) 254–260.
[136] G.Y. Chen, X.Y. Song, T.J. Richardson, Electrochemical and Solid-State Letters 9 (2006) A295–A298.
[137] L. Laffont, C. Delacourt, P. Gibot, M.Y. Wu, P. Kooyman, C. Masquelier, J.M. Tarascon, Chemistry of Materials 18 (2006) 5520–5529.
[138] C. Delmas, M. Maccario, L. Croguennec, F. Le Cras, F. Weill, Nature Materials 7 (2008) 665–671.
[139] G. Brunetti, D. Robert, P. Bayle-Guillemaud, J.L. Rouvière, E.F. Rauch, J.F. Martin, J.F. Colin, F. Bertin, C. Cayron, Chemistry of Materials 23 (2011) 4515–4524.
[140] A. Nytén, A. Abouimrane, M. Armand, T. Gustafsson, J.O. Thomas, Electrochemistry Communications 7 (2005) 156–160.
[141] R. Dominko, M. Bele, M. Gaberšček, A. Meden, M. Remškar, J. Jamnik, Electrochemistry Communications 8 (2006) 217–222.
[142] Z.L. Gong, Y.X. Li, Y. Yang, Electrochemical and Solid-State Letters 9 (2006) A542–A544.
[143] T. Muraliganth, K.R. Stroukoff, A. Manthiram, Chemistry of Materials 22 (2010) 5754–5761.
[144] R.W. Pekala, Journal of Materials Science 24 (1989).
[145] J.A.R.C. Lin, Carbon 38 (2000).
[146] Y.-X. Li, Z.-L. Gong, Y. Yang, Journal of Power Sources 174 (2007) 528–532.
[147] R.K.B. Gover, P. Burns, A. Bryan, M.Y. Saidi, J.L. Swoyer, J. Barker, Solid State Ionics 177 (2006) 2635–2638.
[148] H.J.T. Ellingham, Journal of the Society of Chemical Industry 63 (1944) 125–160.
[149] J.D. Gilchrist, Extracction Metallurgy, 2nd ed., Pergamon Press, 1980.
[150] T.N. Ramesh, K.T. Lee, B.L. Ellis, L.F. Nazar, Electrochemical and Solid-State Letters 13 (2010) A43–A47.
[151] V. Legagneur, Y. An, A. Mosbah, R. Portal, A. Le Gal La Salle, A. Verbaere, D. Guyomard, Y. Piffard, Solid State Ionics 139 (2001) 37–46.
[152] Y.Z. Dong, Y.M. Zhao, P. Fu, H. Zhou, X.M. Hou, Journal of Alloys and Compounds 461 (2008) 585–590.
[153] Y.Z. Dong, Y.M. Zhao, Z.D. Shi, X.N. An, P. Fu, L. Chen, Electrochimica Acta 53 (2008) 2339–2345.
[154] A. Yamada, N. Iwane, Y. Harada, S.i. Nishimura, Y. Koyama, I. Tanaka, Advanced Materials 22 (2010) 3583–3587.
[155] L. Chen, Y. Zhao, X. An, J. Liu, Y. Dong, Y. Chen, Q. Kuang, Journal of Alloys and Compounds 494 (2010) 415–419.
[156] J.C. Kim, C.J. Moore, B. Kang, G. Hautier, A. Jain, G. Ceder, Journal of the Electrochemical Society 158 (2011) A309–A315.
[157] G. Hautier, A. Jain, H.L. Chen, C. Moore, S.P. Ong, G. Ceder, Journal of Materials Chemistry 21 (2011) 17147–17153.
[158] A. Jain, G. Hautier, C.J. Moore, S.P. Ong, C.C. Fischer, T. Mueller, K.A. Persson, G. Ceder, Computation Materials Science 50 (2011) 2295–2310.
[159] T. Mueller, G. Hautier, A. Jain, G. Ceder, Chemistry of Materials 23 (2011) 3854–3862.